Doctoral Dissertation

Research and development on the formation of neuron-microelectrode junction mediated by synapse organizing molecules

Name: Kim Samyoung

Supervisor: Hidekazu Tsutsui

Graduate School of Advanced Science and Technology
Japan Advanced Institute of Science and Technology
[Materials Science]

June 2023

2023/06

Abstract

The nervous system of organisms is a complex system composed of various types of cells forming a neural network that uses electrical signals to control, process, and record the body's activity. Therefore, experiments and analyses on the dynamic flow of these electrical signals are necessary to understand the phenomena occurring in the human body. The study of bioelectricity and electrical properties of living organisms is known as electrophysiology, and the techniques used for such research are called electrophysiological techniques.

Electrophysiology technology using microelectrodes has a limitation in that it cannot selectively target specific types of cells within a variety of cells. These limitations make it difficult to study the functions and roles of specific cells. An optical electrophysiology technique using a fluorescence probe has recently emerged to solve this problem. However, this also has technical limitations. In particular, conventional electrophysiology techniques that can be used together with optical electrophysiology techniques are limited to intracellular recording using patch clamps or Insertion electrodes that damage cells. In addition, it is difficult to accurately measure action potentials solely with optical signals due to the low temporal resolution.

This study was conducted to overcome the limitations of conventional electrophysiology techniques using microelectrodes by using IL1RAPL1 (Interleukin-1 receptor accessory protein-like-1), a type of synapse organizer. Synapse organizers refer to adhesion molecules responsible for synapse formation and induction on the surface of the branch terminals of neurons.

This experiment consists of three chapters. The first chapter demonstrates the process of making the electrode smaller than the area of the axon terminal, as well as the presentation of the process of stably functionalizing the surface of the electrode. In the second chapter, neurons were cultured on the surface of electrodes that had been functionalized with IL1RAPL1, and then the inductive synaptic differentiation between the functionalized electrodes and neurons was confirmed. In the third chapter, based on the information obtained from the fabricated MEAs, simulation was used to test whether action potentials could be measured from neurons. Since the electrodes were smaller than the axon terminal, it was expected that they would induce wrapping from the axon terminal, resulting in the formation of a high Rseal and the ability to measure the action potential of the axon terminal.

Unfortunately, recording action potentials from actual neurons was impossible in this study. However, the experiment demonstrated that the common limitations of conventional electrophysiology techniques using microelectrodes can be overcome. A new technique of introducing synapse organizers into electrodes was proposed and a stable method was established. These findings suggest that in future electrophysiological experiments using microelectrodes, long-term observation and analysis can be achieved through an extracellular recording by selectively targeting specific types of cells. The same lab is also experimenting with making synapse organizers respond to specific targets, which indicates that large-scale parallel measurement through more accurate targeting will be possible in the future.

Finally, this study showcases a novel approach to electrophysiology techniques employing microelectrodes. However, there are still many unfinished aspects left. Although these techniques have

problems, ongoing improvement efforts can address these imperfections. i believe that this novel form of electrophysiology technology has the potential to make substantial contributions to future research in the field.

Keyword: Electrophysiology, Molecular biology, Biosensor, Neuron, Fluorescent protein

Contents

Chapter 1
Introduction

1.1 Electrophysiology

Electrophysiology is a discipline that analyzes and investigates the dynamic flow of action potentials and their role in the excitation and conduction occurring in the nervous system[1]. Essentially, everything that happens in the body is very likely connected in some way to electrical phenomena. Therefore, a thorough understanding of the electrical activity of living organisms is critical to understanding the mysterious phenomena that occur in living organisms. Electrophysiology is the field that delves into this fascinating area, and the techniques used for such research are known as electrophysiological techniques.

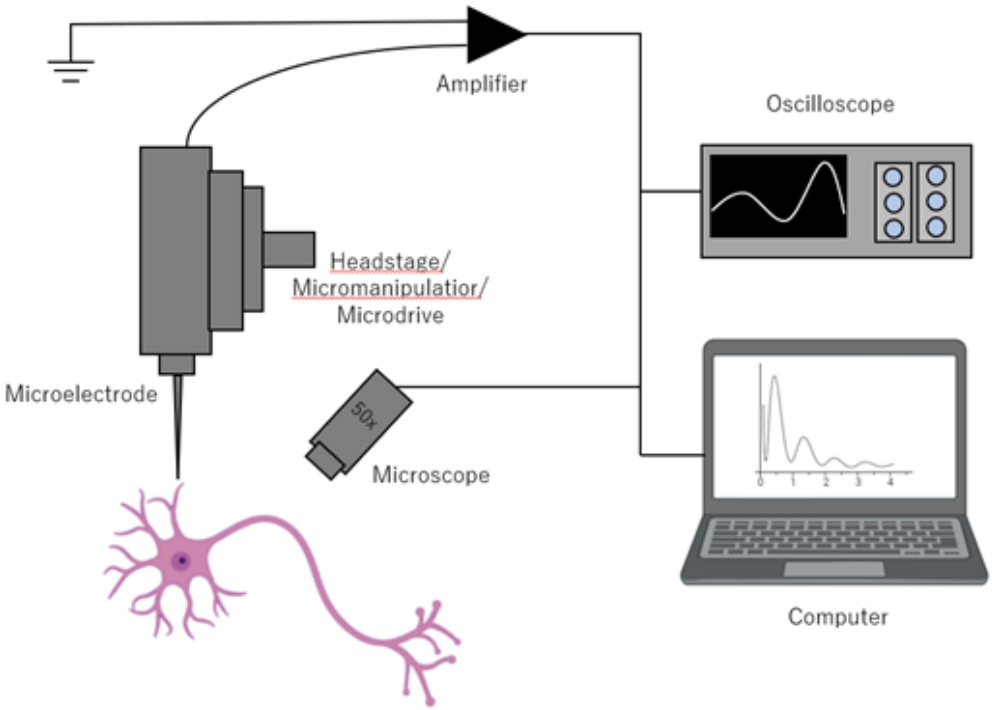

Fig.1. The composition of contemporary electrophysiology.

Electrophysiology, which explores the electrical properties of living organisms, has a rich

history dating back to the 18th century. In 1786, Luigi Galvani made a groundbreaking discovery when he observed a convulsion in a dissected frog leg, realizing it was an electrical event[2]. This observation marked the start of the field of electrophysiology. During the 19th century, notable scientists such as Raymond and Helmholtz built upon Galvani's discovery by studying action potentials in animal muscles, thereby laying the foundation for the development of this field[3][4] [5][6][7][8].

With the advancements in technology in various fields, Electrophysiology has seen tremendous growth in recent times. In particular, advances in various technologies, such as electronics, electrical engineering, material engineering, and image processing, have helped investigate electrophysiology in the broader area. As a result, electrophysiology is being studied in many areas, including neural control mechanisms, biological signals, and brain activation.

Electrophysiology experiments typically involve the control and measurement of voltage or current in cells using electrodes[9][10]. The type of electrode used varies based on the intended purpose of the experiment, and researchers have a wide range of shapes and sizes to choose from. This chapter provides an overview of the basics of neurons and the various electrophysiological techniques used to study them.

1.2 Basic electrical properties of neurons

Animals sustain their lives by consuming food through their mouths, which is then absorbed and broken down by enzymes and chemicals within the body. This process involves various neural mechanisms and demonstrates the interplay of physical and chemical phenomena controlled by the nervous system. The contractile action of muscles during activities such as walking or carrying a cup is also regulated by nerve mechanisms. The nervous system contains many different types of cells, but commands are transmitted and controlled primarily by excitatory cells called neurons[11]. These neurons vary in shape and size depending on their type, but all have a similar basic structure. A typical neuron consists of a nerve cell body, dendrites, and an axon (as depicted in Figure 2). The dendrites are connected to sensory receptors or the axon terminals of other neurons, while the axons are responsible for transmitting action potentials. Communication between neurons takes place through a small cleft known as a synapse, where information is transmitted through the synaptic cleft.

Neurons transmit signals to other cells or store information through either electrical or chemical transmission at synapses. Electrical transfer occurs through the transfer of ions through ion channels, while chemical transmission involves the transmission of a signal through a neurotransmitter.

The membrane of nerve cells is composed of a phospholipid bilayer that separates the inside and outside of the cell, with ion channels such as sodium and potassium channels

expressed on the membrane (as depicted in Figure 2).

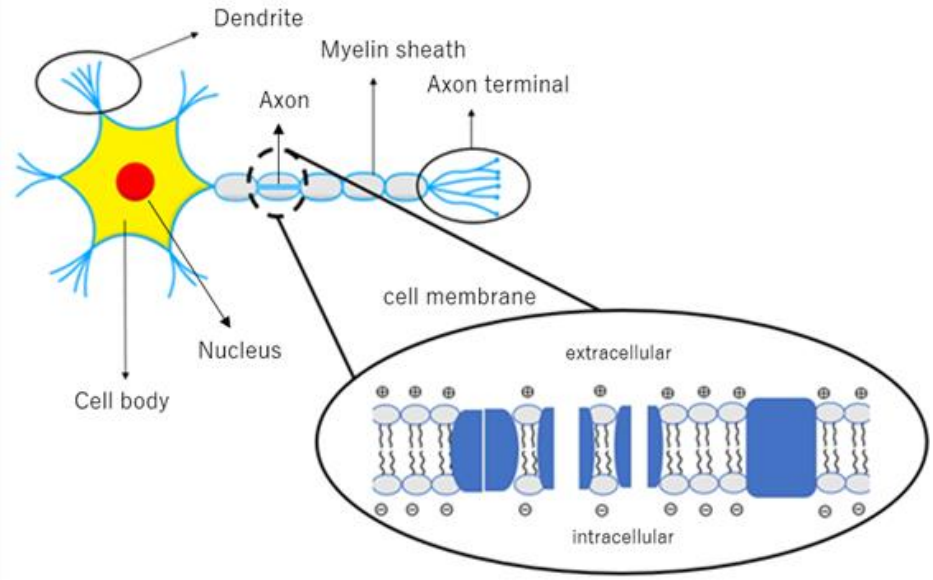

Fig.2. Structure of Neurons

Neurons have different concentrations across the cell membrane. As a result of these differing ionic properties, neurons are considered excitable cells, capable of transmitting signals through the concentration gradients of intracellular and extracellular ions[12]. This creates an electrical gradient, and the principles of signal transduction are based on these physiological mechanisms. In response to excitatory stimuli transmitted from sensory cells or muscle tissue, organisms generate voltage changes, known as action potentials. These action potentials are driven by the movement of ions through ion channels in the cell membrane, with most movement being influenced by the concentration gradient.

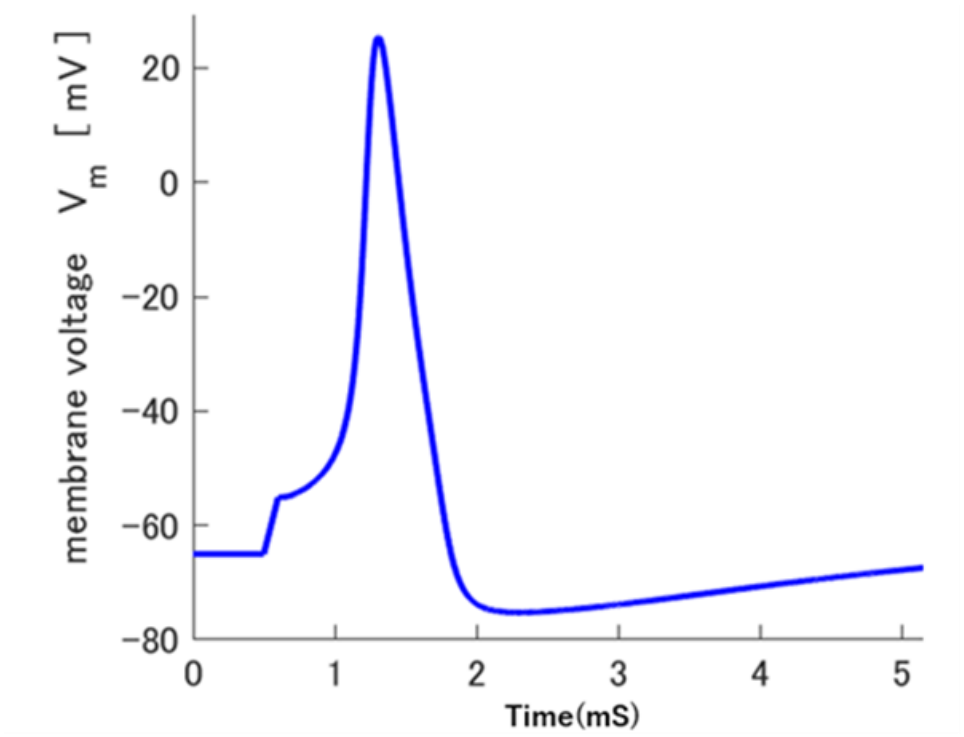

Fig.3. Action potential

The inside of a neuron has a resting potential of approximately -70 millivolts, which is the absence of stimulation from the outside. During this state, called polarization, the sodium (Na+) channels open when a neurotransmitter is transmitted through a synapse. This results in the flow of Na+ ions into the inside of the cell, causing the membrane potential to reverse and the interior of the neuron to become positively charged, known as depolarization. Once the potential in the cell reaches about 30 millivolts, the sodium channels close and the membrane potential stabilizes. At this point, a potential-dependent potassium (K+) channel opens and a significant amount of K+ ions flow out of the cell, restoring the potential to its original state, referred to as repolarization. This is followed by a temporary hyperpolarization, in which the intracellular membrane potential becomes

less than -70 mV.The electric driving force that transmits the stimulus is then generated by the movement of charged particles [12][13][14]. The current generated is referred to as a local current and its shape is fixed, meaning action potentials occur with the same amplitude and time period in any cell. Most local currents transmit excitation at a rate of 1 to 100 meters per second.

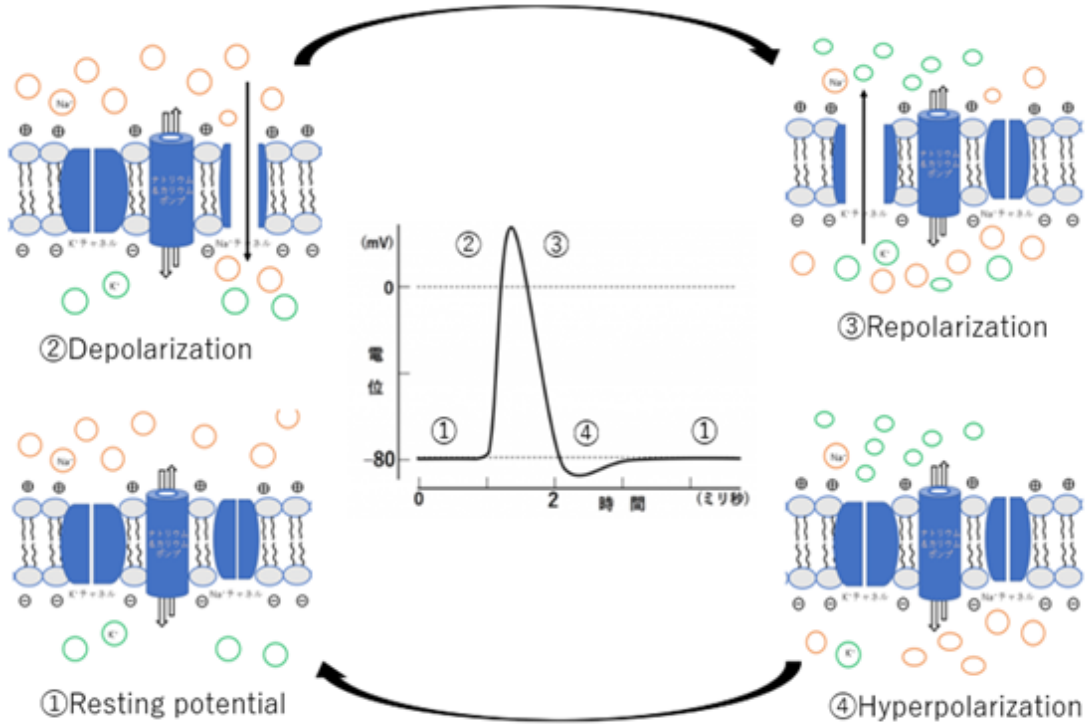

Fig.3. Mechanism of Action potential

Multiple neurons may emit constant action potentials at rates of 10 to 100 times per second, which propagate along the axon to the end of the axon and are transmitted to other neurons through synapses, where they serve as electrical signals [13][14].

1.3 Synaptic

Information transfer between neurons occurs at specialized junctions called synapses. These synapses typically form a gap, referred to as the synaptic cleft, between the pre-synaptic differentiation located at the end of the axon and the post-synaptic differentiation located at the end of the dendrite. The size of the gap varies depending on the type of synapse, with electrical synapses having a cleft of 2 to 3 nm and chemical synapses having a gap of 20 nm.

Synapses can be classified into two types based on the transmission mechanism, electrical and chemical. In electrical synapses, the pre-synaptic and post-synaptic cell membranes are connected by an ion bridge, allowing for direct transfer of information from the pre-synaptic to the post-synaptic neuron. Chemical synapses, which are the most prevalent in the central nervous system, involve the release of neurotransmitters into the synaptic cleft. When an action potential reaches the end of an axon, a potential-dependent calcium channel opens to allow calcium ions into the pre-synaptic terminal, resulting in the release of neurotransmitters. The neurotransmitter then binds to the neurotransmitter receptor protein in the post-synaptic membrane and elicits a change in membrane potential or activates a secondary messenger in the cell, thereby transmitting the information. Synapses can also be categorized into excitatory and inhibitory synapses based on their functions. Excitatory synapses cause excitation in the post-synaptic cell, while inhibitory synapses cause inhibition [6][14].

In addition, to signal transduction receptors, there are several membrane proteins present in synapses that have various functions, such as the formation, maintenance, and induction of synaptic structures. Examples of these proteins include neurolysin, neurexin, and cadherin. These proteins play a crucial role in enabling the formation of synapses at specific locations.

1.4 Basic Techniques of Electrophysiology

The transmission of information within organisms, including various sensory processes, has been found to be an electrical phenomenon based on numerous studies. One notable example is the experiment conducted by Hodgkin and Huxley, who were the first to measure action potentials in the nerve cells of giant squid [15]. Through the use of a glass tube electrode and cell fixation, they established the relationship between membrane potential and ion permeability[9] [12][16] [17].

As technology has advanced, the field of electrophysiology has also grown and diversified. Electrophysiology techniques are broadly categorized into three types based on the location of recording within a neuron cell. These include extracellular recording, intracellular recording, and patch-clamp recording[16][17]. In recent times, advancements in molecular biology and biotechnology have introduced fluorescence-based technologies. Fluorescent probes, also known as fluorescent labels, are used in the detection of biomolecules such as proteins, antibodies, and amino acids. These probes are

highly selective in their binding properties and enable the observation of specific targets with high accuracy.

These techniques provide important information about ionic currents, synaptic transmission, and neural activity in various regions of the nervous system. However, despite their usefulness, there are also limitations and challenges associated with Conventional electrophysiology techniques that should be considered.

1.4.1 Intracellular recording

The intracellular recording is a technique for measuring the electrical activity of cells that was first developed in the 19th century using electrodes and vacuum tubes. Ling and Gerard were among the first to use this method to record vital signals using sharp glass electrodes (Ling & Gerard, 1949) [8][17]. Despite its efficiency in providing high temporal and spatial resolution, as well as allowing for the direct measurement of ionic currents, intracellular recording is an invasive technique that can cause stress or harm to the sample, particularly when the sample is an animal. In addition, the method can be disrupted by external factors such as respiration or pulse, making it challenging to use for long-term observation of live samples and requiring high technical skills and perseverance. Nevertheless, intracellular recording remains an essential tool in electrophysiological studies and is used to observe changes in microscopic membrane potentials, such as post-synaptic potentials and action potentials.

1.4.2 Extracellular recording

Extracellular recording is a technique used to study the electrical activity of neurons in the brain. It has its roots in the late 19th century, when the resting potential of cells was discovered by German physician Carl Ludwig. This discovery led to further studies of the electrical properties of cells, including the signals generated by neurons.

Extracellular recordings have several key properties that make them useful tools for studying the electrical activity of neurons and the communication between neurons. One of the hallmarks of extracellular recording is the ability to measure and record the electrical activity of neurons simultaneously on a large scale. It also provides a high degree of spatial and temporal resolution. This enables the analysis of the interaction of clusters of neurons in the nervous system, and thanks to the high temporal resolution, the timing of action potential firing can be clearly identified. However, extracellular recording also has its limitations. One drawback of extracellular recording technology is that voltages below about 1 mV are generally difficult to detect. Additionally, it does not enable the recognition of a single cell but rather simultaneously records multiple waveforms surrounding it. As a result, after recording multiple waveforms, the activity of each cell is distinguished by the difference in size or shape of the waveforms, making it challenging to target and record single cells. Despite these limitations, extracellular recording is widely used in many studies due to its many advantages. An example of the advantage of extracellular recording using electrodes is that long-term observation is possible because the cells are minimally stimulated[7][8][18][19].

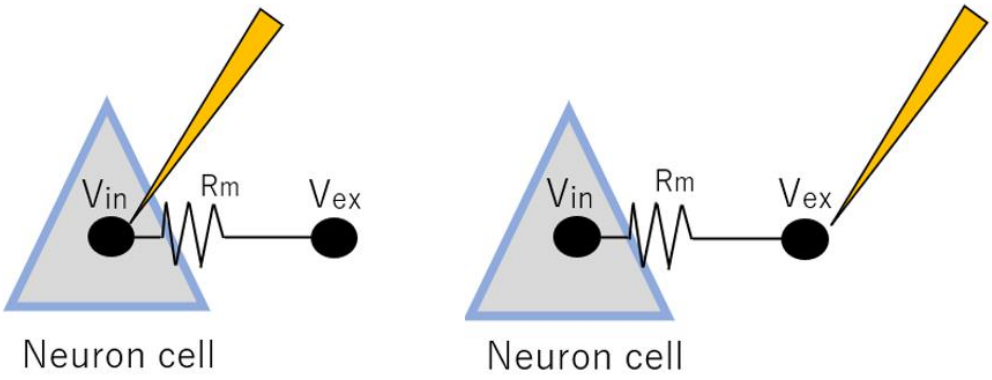

Fig.4. The left represents Intracellular recordings, and the right represents Extracellular recordings.

1.4.3 Patch Clamp

The Patch Clamp technique is a widely used electrophysiological method that enables researchers to study the properties of individual cells in a controlled and precise manner. Developed in the 1970s by German biophysicist Erwin Neher and British biophysicist Bert Sakmann, the technique has since become an essential tool in cellular and molecular biology and has played a critical role in our understanding of cell function and signaling. The basic principle of the Patch Clamp involves the use of a small glass micropipette, known as a patch electrode, which is placed close to a single cell to form a high-resistance seal between the pipette tip and the cell membrane. This allows researchers to measure the electrical signals generated by the cell with high precision. The Patch Clamp technique can be used to study a wide range of cellular processes, including ion channels,

neurotransmitter release, and the electrical activity of neurons[20].

There are several modifications of the basic Patch Clamp technology that can be applied depending on the research purpose, including cell-attached patch, inside-out patch, whole-cell recording, outside-out patch, and perforated patch. The cell-attached patch allows for the recording of single ion channel currents or nerve cell firing frequency without altering the intracellular environment, while the inside-out patch involves separating the patch membrane from the cell. Whole cell recording involves breaking the cell membrane to connect the inside of the electrode and the inside of the cell, while the perforated patch involves creating a small hole in the cell membrane using an antibiotic in the patch electrode solution. (Fig.5)

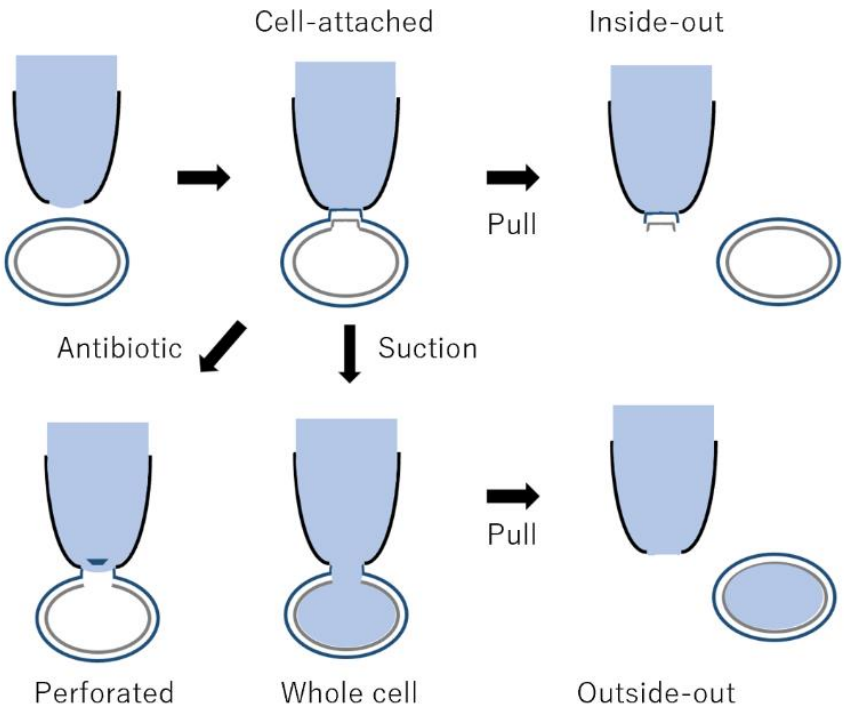

Fig.5. Types of Patch Clamp Technology: Cell-attached: This method involves recording the current through an ion channel after sealing the pipette to the cell

membrane to prevent damage to the cell membrane. Inside-out: This method involves extracting the cytoplasm near the cell membrane using a pipette to examine the components of the cytoplasm. Whole-cell: This method involves rupturing the cell membrane using a pipette to integrate the inside of the electrode with the inside of the cell. It is primarily used to observe changes in real-time after administering a reagent. Outside-out: this method primarily extracts intracellular blisters and moves them or observes changes in ion channels caused by reagents (Similar to the inside-out method.). Perforated: Unlike other methods that use suction to damage cell membranes, this method uses reagents to remove cell membranes.

One of the key advantages of the Patch Clamp technique is its high level of control and precision, allowing researchers to selectively target specific sub-cellular structures and control the composition of the intracellular and extracellular fluid. This feature is essential for studying the electrical properties of cells under controlled conditions. The technique also has the ability to measure the electrical signals generated by individual cells, making it crucial for understanding the electrical properties of neurons and cell-cell communication pathways.

However, the Patch Clamp technique also has some limitations. It is a time-consuming process that can take several minutes to form the seal and several hours or days to measure the electrical signals. Additionally, it is not well-suited for studying the function of cells in tissues or organisms and is difficult to use on small cells due to the lack of cell-specific selectivity. Despite these limitations, the Patch Clamp technique remains an important tool for researchers across various fields, and its continued development and improvement is expected to play a crucial role in advancing our understanding of cellular function and signaling.

1.4.4. optical electrophysiology

Optical electrophysiology is a technique used to measure the electrical signals generated by biological cells and tissues. This is accomplished through the use of optical probes, such as voltage-sensitive dyes or genetically encoded voltage indicators, that fluoresce in response to changes in the cell membrane potential. By detecting changes in fluorescence, researchers can measure changes in membrane potential and, therefore, the electrical activity of the cell. Additionally, optical electrophysiology provides real-time observation of cellular electrical activity, enabling the study of dynamic electrical signaling in biological systems. The discovery of fluorescent protein in jellyfish by Osamu Shimomura in 1960 has led to tremendous advances in biotechnology, making it an indispensable material today. In the 1970s, fluorescent proteins were first applied to electrophysiology by Larry Cohen and colleagues at Yale University. Unlike traditional electrophysiology techniques, such as patch clamping, optical electrophysiology does not alter or damage the electrical properties of the cell, making it a valuable tool for the study of living cells.

Conventional electrophysiology techniques can be challenging in distinguishing and recording the activity of specific individual cells, but this issue can be resolved through the use of fluorescent probes in optical electrophysiology. These probes have a high selective binding rate with the target, making them useful for research on specific single cells.

However, optical electrophysiology also has several disadvantages. One of its primary limitations is its reliance on optical probes, which can have limited selectivity and availability. Additionally, optical signals can be easily disturbed by light scattering, absorption, and reflection, leading to measurement errors and limited temporal resolution. Photobleaching can also occur, causing a decrease in the fluorescent signal over time and making it difficult to obtain long-term recordings. In conclusion, despite its limitations, including limited temporal and spatial resolution and the need for extensive training to interpret results, optical electrophysiology remains a valuable tool for the study of cellular electrical activity.

1.5 Goal of study

Organisms receive external stimuli through a network of neurons to learn, remember, and control all body activities, including human body movement, organ function, and metabolism. To understand these neuron systems, various electrophysiological techniques have been developed[21][22][23]. The first use of microelectrodes in brain research was by Renshaw and Morrison in 1940 [24]. They used relatively large microelectrodes and were able to record electrical phenomena from a limited area, demonstrating the potential for experiments in organisms using electrodes. Over time, microelectrodes have improved and now even nano-sized electrodes can be used. Nevertheless, electrophysiology techniques using microelectrodes have not changed much over the past 20 years, and their

limitations are becoming increasingly clear.

Conventional electrophysiology techniques for examining the activity of neurons in the nervous system can be divided into three types: intracellular recording, extracellular recording, and patch clamp. Extracellular recording techniques have excellent recording stability but can only record field potentials from cell membranes and are not suitable for recording very small potentials. Additionally, they cannot selectively contact single cells. Intracellular recording techniques can directly observe changes in small potentials, such as postsynaptic potentials, but cause damage to the cell as the electrode must be inserted into it. The selectivity of the intracellular recording technique is often lost due to various external factors, a problem also observed in the patch clamp technique. The perforated patch technique allows for longer observation periods than conventional extracellular recording, but the observation period is still shorter due to cell self-repair and apoptosis caused by damage. Recently, optical technologies using fluorescent probes have gained attention. The fluorescence probe technique is often used in experiments requiring high selectivity and can allow for long-term observation without causing damage to cells. However, the fluorescence probe technique has lower temporal and spatial resolution than conventional electrophysiology techniques.

Electrophysiology technology using microelectrodes has a limitation in that it cannot selectively target specific types of cells within a variety of cells. These limitations make it difficult to study the functions and roles of specific cells. To address this issue, photo

electrophysiology techniques using fluorescent probes have emerged. However, these techniques also have limitations. Therefore, this study presents a novel approach utilizing IL1RAPL1(Interleukin-1 receptor accessory protein-like-1), a type of synapse organizer, to endow microelectrodes with the ability to target specific types of neurons selectively.

In this study, MEAs (Microelectrode Arrays) were mainly used. MEAs are utilized for extracellular recordings and can increase seal resistance without damaging sample cells [25]. In particular, they allow for massively parallel measurements. By introducing cell-specific binding properties to MEAs, we aim to achieve stable and selective recording.

Chapter 2 studies the fabrication of MEAs and protein adsorption on electrode surfaces. Many labs are experimenting with adsorbing proteins onto solid surfaces, with most experiments focusing on the adsorption mechanism and increase. Most protein adsorption technologies using electrical phenomena use DC voltage, but it has been reported that electrical repulsion between proteins occurs when proteins are adsorbed using DC voltage, leading to low uniformity and hindering protein adsorption. In my experiment, it is crucial to adsorb a uniform amount of protein with a high success rate.

To address the problem of DC voltage, i have decided to use pulse-type voltage. In this chapter, I use pulse-type voltage to demonstrate the repulsion between proteins that occurs with a DC voltage and suggest a better electrical protein binding method. This study on protein adsorption will be useful for future studies that require control over protein adsorption.

Chapter 3 is the central study. I will use a synapse organizer for my new electrophysiology technique by introducing it to the electrode surface to induce specific neurons. I will use is the synapse organizer of IL1RAPL1 (Interleukin-1 receptor accessory protein-like-1). IL1RAPL1 induces RPTP (receptor-type protein tyrosine phosphatases)-bearing axons and forms synapses. The R8 type of the IL1RAPL1 group has an Arg-Gly-Asp-Ser (RDGS) adhesion recognition molecule and induces cell-specific binding with the PTPδ factor in the family of RPTP. Our study aims to induce cell-specific binding with axons that have the PTPδ factor by adsorbing R8, a synapse organizer, onto the electrode. This will lead to the formation of synapses between the axons and the electrodes, and we anticipate that action potentials can be measured within the synaptic space once synapses have formed. This is a novel type of electrophysiology technique and may have problems that we are not yet aware of. Nevertheless, it is believed that this new technique will make a significant contribution to the field of electrophysiology.

In Chapter 4, the MEAs introducing the new electrophysiology techniques will be evaluated through simulation. Developing new technology takes time and money, especially in the case of biological experiments. That's why i plan to use simulation to save time and money. Additionally, the simulation results will allow me to address any problems in this study and determine the direction for future research.

Extracellular recording	Intracellular recording	Patch Clamp	Optical electrophysiology techniques
Multiple	single	single	both possible
long	short	medium	long
medium	High	High	High
High	High	medium (patch-clamp has limited spatial resolution. But temporal resolution is High)	medium (Optical techniques has limited temporal or spatial resolution.)
medium	High	High	optical detection of neuron signals is easily contaminated
Non	Non	Non	High

Table 1. It displays the advantages and disadvantages of each electrophysiology recording method.

Chapter 2 Fabrication of MEAs and functionalization of electrodes

2.1 Introduction

2.1.1. Understanding and Fabrication of MEA

MEAs (Microelectrode Arrays) are submicron-sized electrodes used to study microscopic biological materials, such as DNA, proteins, or cells. The first report of MEAs was by Ida Henrietta Hyde, A female physiologist, in 1857 [26]. MEAs utilize semiconductor microprocessor technology to produce submicron patterns and can record action potentials or change in electrical activity in nerves and muscles. As a result, they have been used in the field of neuroscience for purposes such as controlling cell growth, constructing artificial neural networks, applying electrical stimulation, and observing cell activity[27][28].

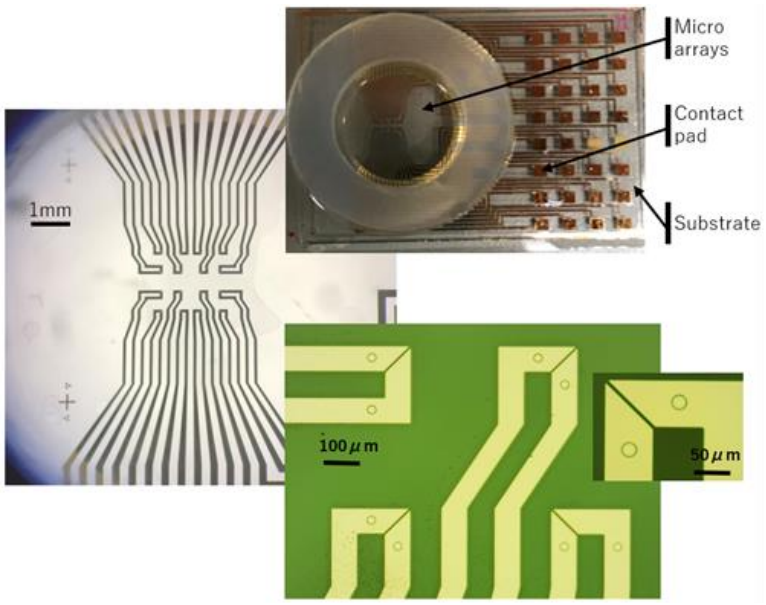

Fig7. The Basic Structure of Microelectrode Arrays (MEAs)

Microelectrodes are mainly divided into two types: invasive and non-invasive. Invasive

electrodes are inserted into cells or tissues to observe the activity of organisms, while non-invasive electrodes can obtain information from the sample's surroundings and surface. Both types of electrodes have their own unique characteristics and are used differently. Although microelectrodes have numerous possibilities, fabrication is not straightforward [28][29][30].

The fabrication of these electrodes requires precise control. Currently, micro-sized electrodes are manufactured through sputter deposition or photolithography, the same process used to make semiconductors. The MEAs used in this study were also fabricated through sputter deposition and photolithography. As a result, this chapter will briefly introduce sputter deposition and photolithography.

1) Sputtering deposition

Sputter deposition is a technique for coating the surface of a substrate without exposing it to liquids or high-temperature gases. It involves the use of an electrically excited gas plasma. First, an inert gas (typically Argon) is injected into a vacuum chamber. Then, a negative voltage is applied to a target, which is the film-forming material. A positive voltage is then applied to the substrate to generate a glow discharge. The inert gas atoms are ionized and collide with the target surface at high speed, causing particles (atoms and molecules) of the target to be expelled. These particles are then deposited on the substrate (such as a silicon wafer or metal wafer) due to electrical attraction. This method is also referred to as the physical vapor deposition (PVD) method.

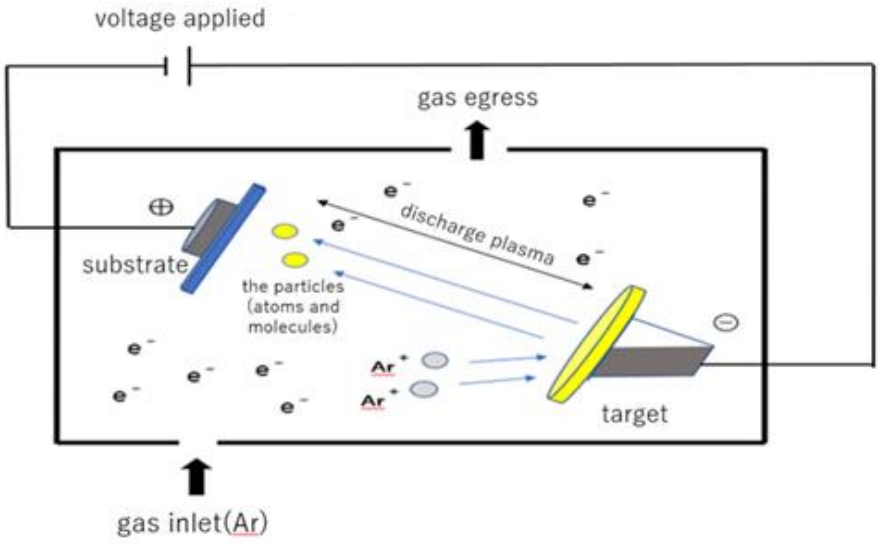

Fig.8. Deposition principle of sputtering

2) Photolithography

Lithography is a technology that transfers circuit patterns onto a substrate using light or electron beams. Photolithography is a technique that transfers patterns using light, primarily ultraviolet light[31]. Before performing photolithography, the wafer is coated with a light-sensitive chemical known as a photoresist. A resist is a material used to form a protective film.

Photoresists are divided into two types: negative and positive, depending on the method of light exposure. In positive photoresists, the part exposed to light is dissolved by a developer. In contrast, in negative photoresists, the region exposed to light becomes solid, while the developer dissolves the parts not exposed to light. In this study, both negative and positive types of photoresists were used.

2.1.2. Understanding Protein Adsorption on Solid Surfaces

The adsorption of proteins onto solid surfaces can occur both naturally and artificially. Many laboratories are conducting research on this phenomenon, such as for the development of biosensors, intra- and extracorporeal devices, protein analyzers, etc. However, the underlying principle of protein adsorption on solid surfaces has not yet been fully understood [32][33][34]. This is due to the complex structural and functional properties of proteins, which are composed of 20 naturally occurring amino acids.

One of the most commonly used methods for attaching proteins to solid surfaces is SAM (self-assembled monolayer) technology, which involves chemically adsorbing organic molecules onto a solid surface using an organic molecular solution[35][36]. Other adsorption methods are the use of temperature, pH, and ion concentration[37]. For example, the temperature method uses high temperatures to increase entropy generation in proteins, leading to increased adsorption, while the pH and ion concentration method changes the balance of positive and negative charges on the protein surface, inducing electrostatic bonding with the target protein.

In this study, an electrostatic attachment technique using pH was introduced to functionalize a specific electrode site. This technique utilizes the protein's isoelectric point (pI), which determines the charge of a protein based on the ionization of an amino group (NH_3^+) and a carboxyl group (COO^-). The pI is the pH at which the average charge of the polyprotic acid becomes zero. If the pH is less than the pI, the protein is positively

charged, and if the pH is higher than the pI, the protein is negatively charged[38][39][40].

Most electrostatic protein adsorption experiments use direct current (DC) voltage. However, it has been reported that this can lead to repulsive forces between proteins during adsorption, making it difficult to control. Therefore, in this study, an attempt was made to control protein adsorption using a pulse voltage. The study aimed to conduct protein adsorption control studies simultaneously in order to achieve an even amount of protein binding within a limited space. However, studies on the control of protein adsorption are inadequate and there is no established standard for the type of voltage applied. This study is expected to contribute to the understanding of the control mechanism of protein adsorption through the use of electrostatic techniques.

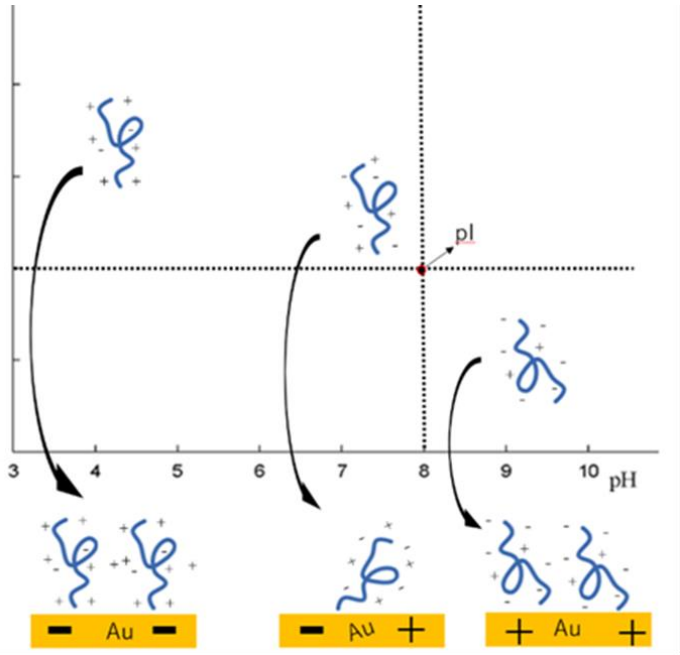

Fig.9. Electrostatic Protein Adsorption Based on the pI-principle.

2.2 Experiment

2.2.1. MEAs fabrication

1.Sputter deposition

Before fabricating MEAs, it is necessary to form a metal film on the substrate, which is a slide glass. The formation of the metal film is accomplished using a sputter deposition device, and in this experiment, the EIS-220 ELIONIX is used. The target metal materials are Cr and Au, which are mounted on the sputter deposition device. Cr and Au are the target metal materials used in the deposition, with Cr deposited first for 20 minutes and Au deposited second for 40 min.

2. Photolithography

The photolithography process involves three steps: photomask fabrication, Au pattern fabrication, and Su8 pattern fabrication. The photomask is fabricated using a laser exposure installation (MLA 150 Advanced Maskless Aligner), which draws a pattern based on CAD data.

The photomask is made on a glass substrate composed of CrO/Cr/CrO/SiO2 and is coated with TSMR (positive photoresist). After being coated with TSMR, the substrate pattern is drawn by the laser exposure installation. The pattern is then developed with the positive developer NMD-3 (2.38%), and Cr is etched on non-photoresist areas. The photoresist is then removed with Remover-1112A.

The Au pattern is fabricated on the substrate with Cr and Au deposited, using a UV exposure installation (UV-Lithography MA-10B Nikon). S1818 (positive photoresist) is

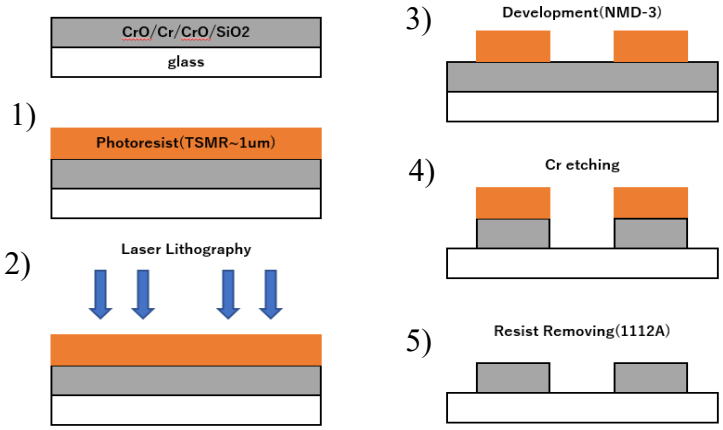

Fig10. Photomask fabrication process

coated on the substrate, followed by pre-baking and exposure to 150 mJ/cm2 by UV exposure installation. The pattern is developed using the positive developer NMD-3 (2.38%), and Au and Cr are etched on non-photoresist areas. The photoresist is then removed with Remover-1112A.

The pattern is developed by the positive type developer NMD-3 (2.38%). Next, cr-Etching is used to remove Cr on non-photoresist areas. Finally, remove the photoresist by Remover-1112A.

The Su8 pattern is fabricated using a negative photoresist (Su8-3005). The surface of the Au pattern is coated with Su8-3005 and subjected to pre- and post-baking. The substrate is then exposed to 100 mJ/cm2 by UV-Lithography, and unsolidified areas are removed with the Su8-Developer solution. Finally, the electrode is washed with IPA and hard-

baked at 200℃ for 10 min.

The next step after the electrode fabrication is to create a bath to hold the solution. This is done using PDMS, a glass ring, and a plastic dish.

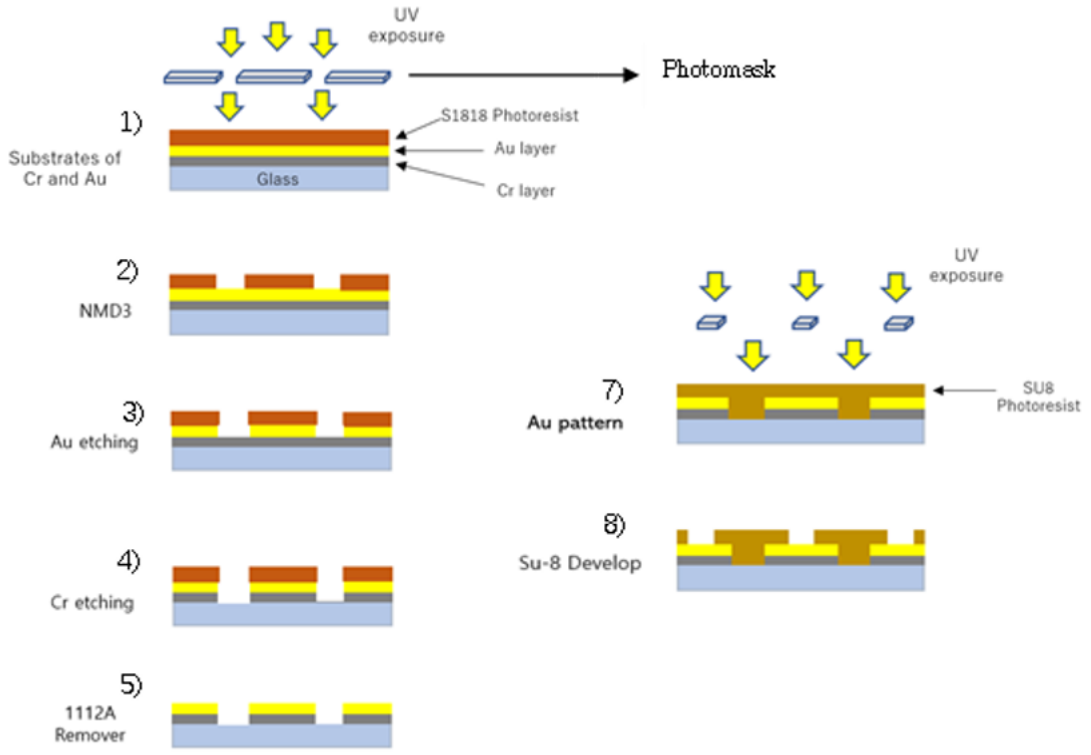

Fig11. The electrode fabrication process

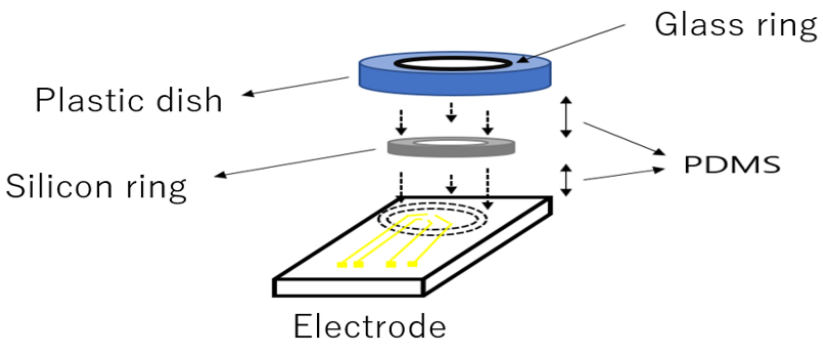

Fig12. Bath fabrication of electrodes

2.2.2 Protein Adsorption Using Electrostatic Technique

1. Evaluation of Protein Adsorption Using Electrostatic Technique

In this chapter, an electrostatic technique is used to attach proteins to the electrode surface. However, the effect of the type of voltage applied on protein attachment using an electrostatic technique is not yet fully understood. Therefore, this experiment aims to observe how protein adsorption is influenced by both DC and pulse voltage. Pulse voltage refers to applying a voltage at regular intervals, while DC voltage refers to applying a constant voltage.

To evaluate protein adsorption, we first fabricate an electrode with a small Su8 chamber. The Source Measure Unit (SMU) device applies voltage and current (using a Newark Source Meter Keithley 2400), while the PWM voltage control device converts the applied voltage into pulses. In this experiment, fluorescent proteins are used, and the fluorescent protein solution is prepared by adding 1 ul of Venus fluorescent protein (concentration unknown) and 1 ul of 1M NaCl to 100 ul of 20mM Hepes 9.0ph, and mixing. 20mM Hepes 9.0ph is prepared by adding 5 ml of 0.2M Hepes Ph9.0 and 250 ul of 10% TritonX to 50 ml of pure water. Before adding the fluorescent protein solution to the Su8 chamber, the electrode surface is cleaned with plasma and UV.

The pulse data for the experiment includes 200 pulses at 25ms intervals, 100 pulses at 50ms intervals, 50 pulses at 100ms intervals, 20 pulses at 500ms intervals, and DC (no pulse). The voltage applied is 1.5V, 1.6V, 1.7V, 1.8V, 1.9V, and 2.0V, respectively. The

fluorescent protein solution is added to the Su8 chamber, and voltage and pulses are applied. After applying the voltage, the adsorption of proteins on the electrode is confirmed using an optical microscope.

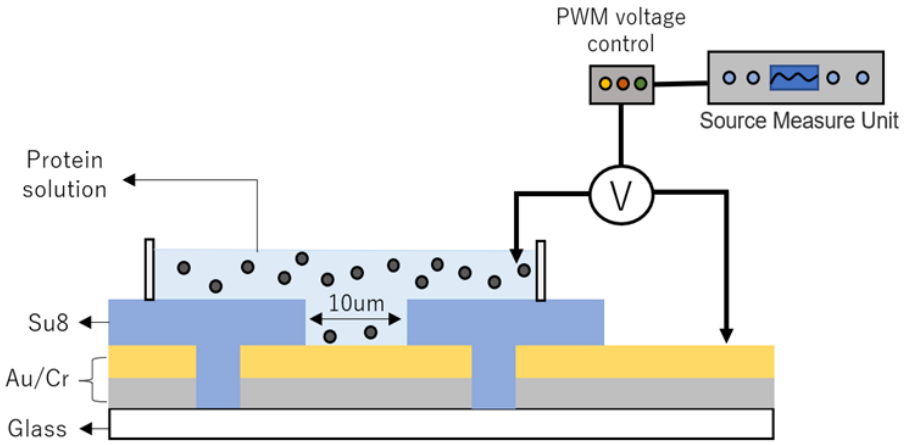

Fig13. Bath fabrication of electrodes

Setting section		**set value**
Source Settings	Source mode	Voltage Bias
	Voltage Level	1.5-2.0V
	Voltage Range	20.0V
	Current Limit	0.0001
	Measurements	500
	Delay	0.0001
Measure Current	Range	100uA
	Min Auto Range	1uA
Measure Voltage	Type	Measured
Measure Resistance	Range	Auto
	Min Auto Range	200

Table 2: Settings Data for the Newark Source Meter Keithley 2400

2.3 Result

2.3.1. MEAs fabrication

1. Sputtering deposition

The sputtering deposition was performed using Cr for 20 min and Au for 40 min, as shown in Fig 14-A. Fig 14 B and C show the target plates used.

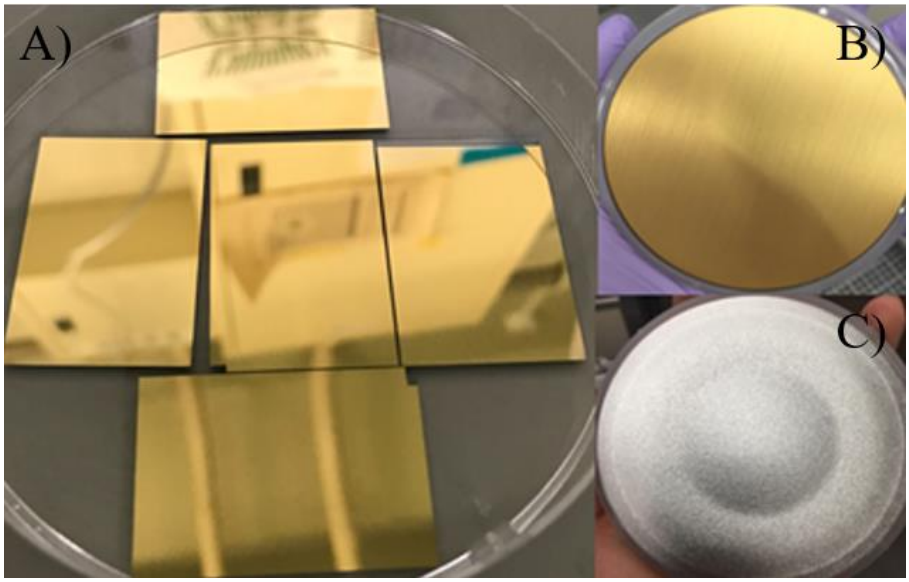

Fig.14. Materials and finished substrates used for sputter deposition.

The thickness of the Cr layer is approximately 0.1um, and the thickness of the Au layer is approximately 0.2um. The average thickness of the substrate after deposition is around 0.3um, which was measured using a KLV Tencor D-500 (Fig. 15).

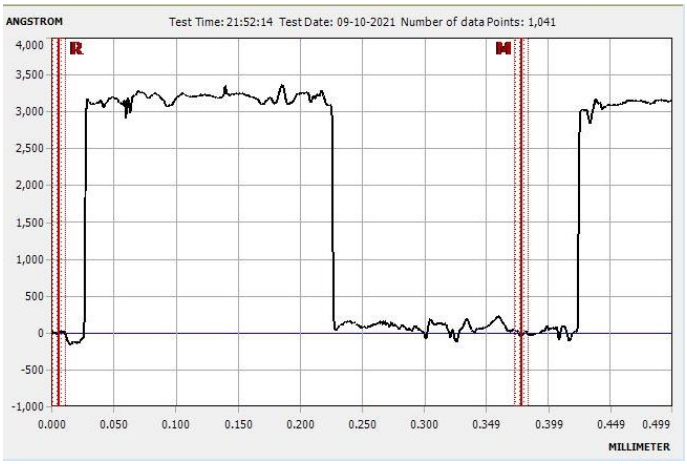

Fig.15 KLV Tencor D-500

2. Photolithography

The design of each Au pattern and Su8 pattern is shown in Fig. 16. A total of six designs were used. The design program used was RAPIDPRO17. Designs A to D were used for neuronal experiments, while designs E and F were used for protein adsorption experiments and the analysis of protein amount. A, C, and E are the mask designs of Au patterns. B, D, and F are the mask designs of the Su8 pattern, with B corresponding to A, D corresponding to C, and F corresponding to E.

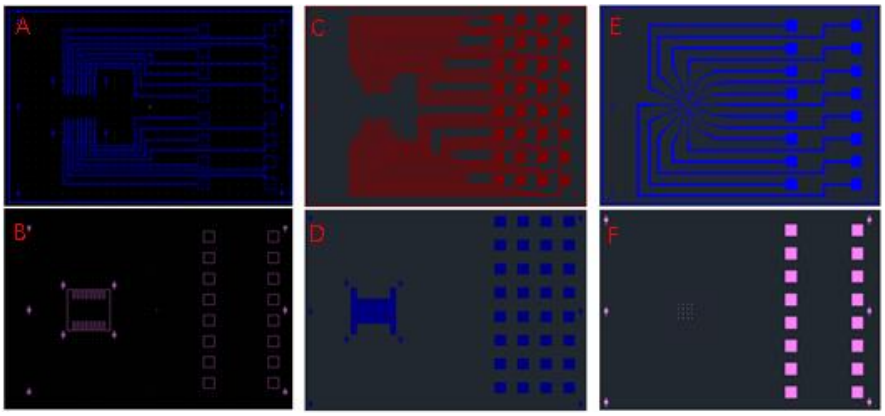

Fig. 16. In this study, design groups A and B were referred to as "16Snake." Design groups C and D were referred to as "32MicroSnake." The designs of E and F were referred to as "16Dot."

Figure 17 is a photomask fabricated based on the design data in Figure 16.

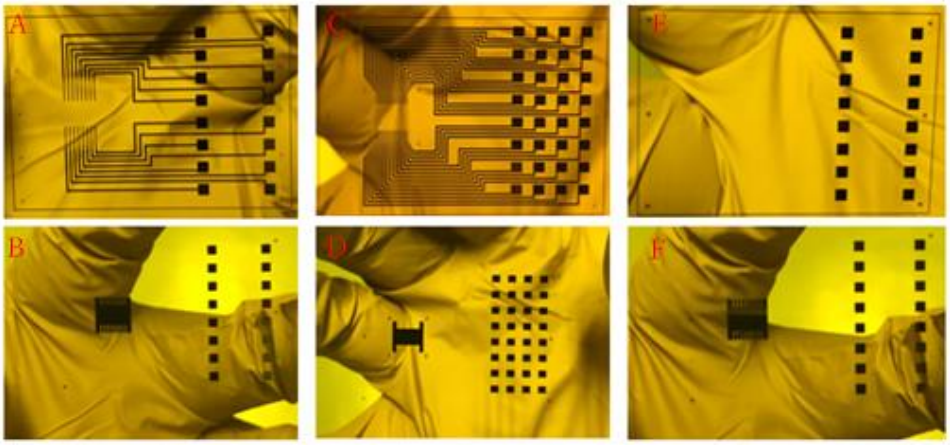

Fig. 17. This figure depicts a photomask constructed based on the design data presented in Fig. 16.

The fabricated masks were used to create electrodes, as shown in Fig. 19.

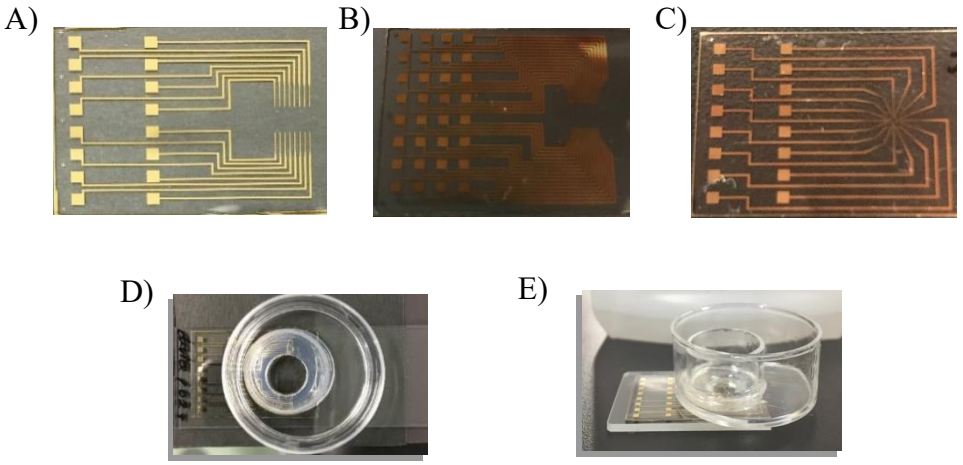

Fig.19. illustrates the Au patterns of the three different design groups, with A representing the 16Snake group, B representing the 32MicroSnake group, and C representing the 16 Dot group. Additionally, D shows the top view of the electrode, and E shows the side view of the electrode.

The 16Snake electrode is a previously used type of electrode, while the 32MicroSnake electrode is the latest type of electrode manufactured through improvement of the 16Snake design.

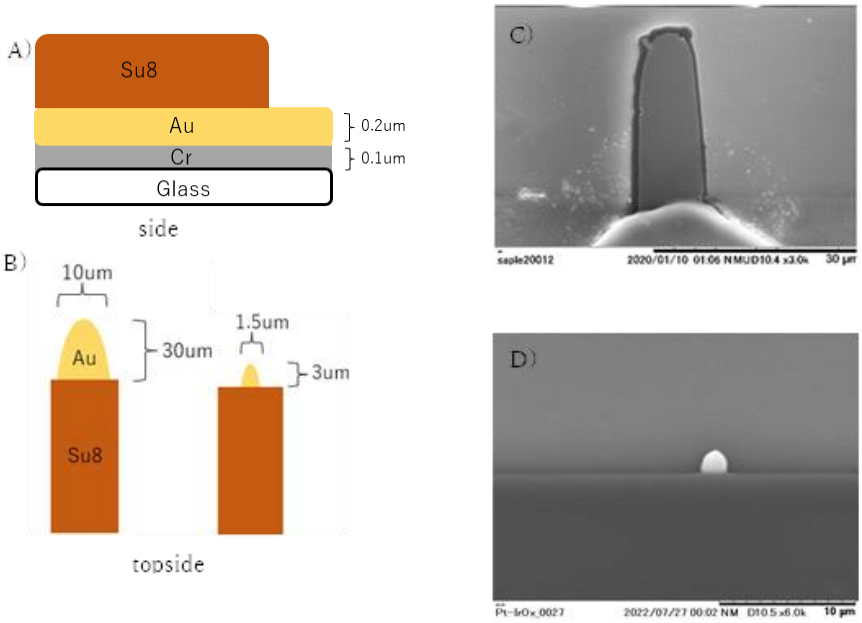

Fig.20. A) This indicates the side view of the electrode configuration. B) This is shown by comparing the electrode sizes of 16Snake and 32MicroSnake. C, D) C is the 16Snake electrode observed using SEM, and D is the 32MicroSnake electrode observed using SEM.

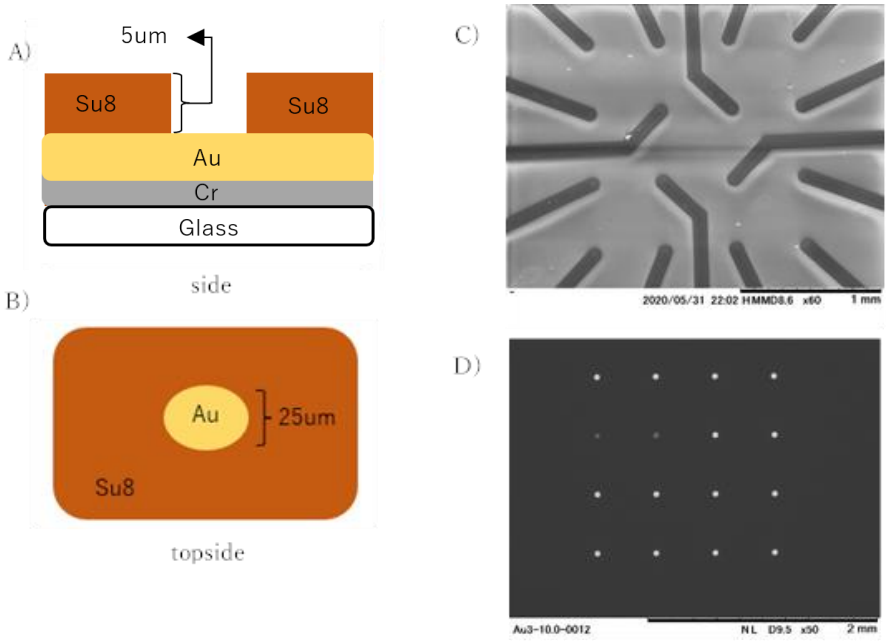

Fig. 21. This figure displays a 16 Dot-type electrode. A) This indicates the side view of the electrode configuration. B) This is a top view of the electrode surface. C) This shows the electrode surface observed by viewed by SEM. D) This shows the electrode surface observed by an optical microscope.

Fig. 20 and 21 show the structures of the electrodes. Fig. 20 displays the structure of the electrodes used in the neuronal cell binding experiment. The height of the electrode is approximately 0.3um. Fig. 20-B on the left side shows the electrode fabricated at the start of the experiment, while the right side of Fig. 20-B displays the electrode that has been reduced in size as much as possible from the initial electrode. The width is 1.5um and the length is 3um, yielding a surface area of 4.5um^2. The width of the synaptic space formed between two nerve cells is roughly 1um to 2.5um, suggesting that the synaptic space can encompass the electrode. These small electrodes are currently the ones being used.

Fig. 21 represents the electrode used in the protein adsorption experiment. A small chamber is visible on the surface of the Su8 pattern that is formed along the electrode. The height of the chamber is around 5um and was utilized in both the protein adsorption experiment and the experiment to determine the amount of adsorption.

In conclusion, all electrodes fabricated by me possess the characteristic of micro multiple arrays.

2.3.2. Evaluation of Protein Adsorption

In this study, I investigated the effect of the type of voltage applied on protein adsorption. I used Venus protein, a fluorescent protein, to observe the adsorption process. The electrode used in the experiment was one with a small chamber on the surface of the Su8 pattern. I attempted to perform protein adsorption on the electrode surface using voltages

ranging from 1.5V to 2.0V, but I could only obtain data at 1.9V.

A)

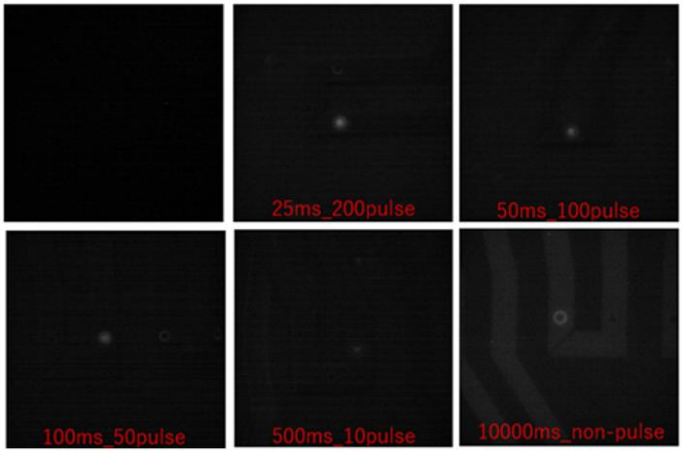

B)

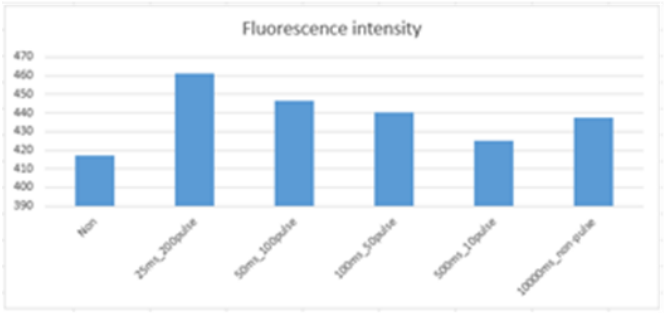

voltage type	Fluorescence intensity
Non	417.071
25ms_200pulse	461.273
50ms_100pulse	446.467
100ms_50pulse	440.092
500ms_10pulse	425.296
10000ms_non-pulse	437.372

Fig. 22. It shows the results of confirming protein adsorption. Panel A shows the Venus protein adsorbed based on changes in pulse voltage, and Panel B shows the individual fluorescence intensities.

Fig. 22-A shows the result of observing Venus attached to the electrode surface after 1.9V was applied. The total duration of the experiment was approximately 10 sec, which was nearly the same for all experiments (Refer to Fig. 23). Fig. 22-B shows the result of fluorescence intensity measurement using HCImageLive. Fig23 shows the state of the

current flow of each pulse when voltage is applied.

The highest fluorescence value was observed when 200 pulses were applied at 25 ms intervals, as indicated by the numerical values in Fig 22-B (The time of the voltage not applied is equal to the time of the voltage application.). The fluorescence intensities observed at 50ms and 100ms are almost identical, but a slightly stronger intensity was observed at 50ms. On the other hand, the lowest fluorescence value was observed when 20 pulses were applied at 500 ms intervals.

I discovered that the number of pulses has a more significant impact on protein adsorption than the length of time the voltage was applied, as shown in Fig.22 and Fig.23.

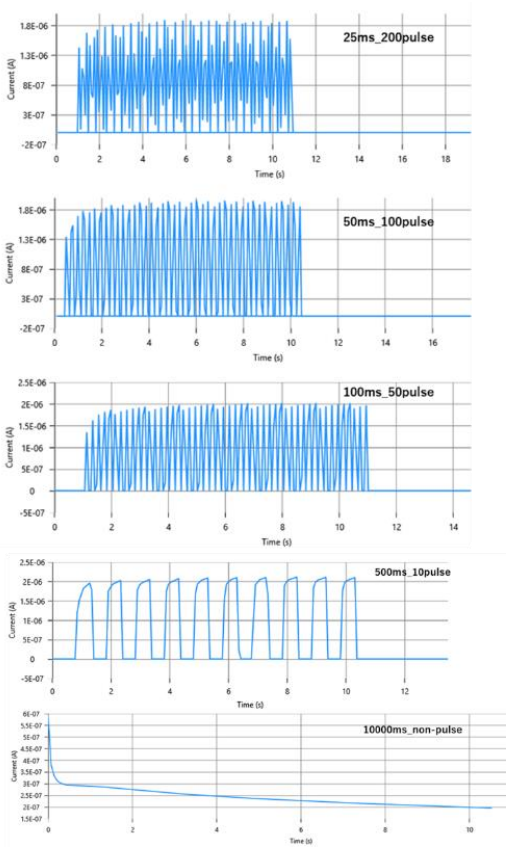

Fig.23. It shows the state of voltage-current according to each voltage application type.

2.4 Discussion

2.4.1. MEAs fabrication

My initial electrodes were larger than the size of the synapse formation. However, after much effort, I reduced the electrode to a size smaller than the size of the synapse formation.

2.4.2. Evaluation of protein adsorption

I investigated the relationship between the type of voltage applied and protein adsorption. Fig.22 and 23 shows that the number of pulses has a greater impact on protein adsorption than the duration of applied voltage.

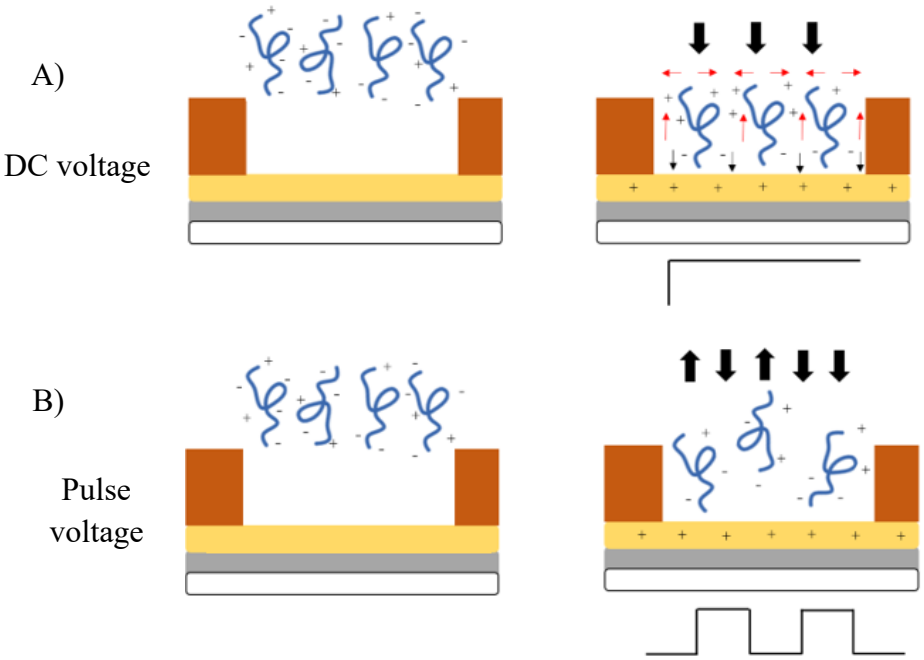

Fig. 24. This shows the direction of action of the repulsive force, assuming that an electrostatic repulsive force arises between proteins when a voltage is applied.

Fig 24-A shows the coupling environment when a DC voltage is applied. When a direct voltage is applied, proteins move toward the electrode in the same direction. At this time, domains with the same potential and direction will aggregate, resulting in a repulsive force between domains. It is speculated that this repulsive force disrupts the binding between the protein and the electrode. On the other hand, when the pulsed voltage is applied in Fig. 24-B, there is a section in which no current flows and it is assumed that the protein turns in the safest direction during the no-current flow period. The reduced repulsion force between the proteins is estimated to enable more stable binding under pulsed voltages (This result shows that the time interval between the application and non-application of voltage is equal. Therefore, it can also be considered that the frequency of non-application of voltage has a more significant effect on protein adsorption than the duration of non-application.).

On the other hand, fluorescence was only observed at the outer corners of the chamber when DC voltage was applied. This result was unexpected and was thought to be due to the strong repulsive force between proteins causing polarization, resulting in protein adsorption only at the edge where the repulsive force was relatively weak.

However, further experiments have shown that these results are due to the generation of air bubbles. This was more clearly observed at higher voltages. This indicates that protein adsorption using electrostatic methods is also affected by factors other than the repulsive force between proteins.

In conclusion, my experiment showed that more stable binding is possible under pulsed

voltage than under DC voltage, but uniform protein binding remains difficult, even with pulsed voltage. This is presumed to be attributed to factors other than the repulsive forces between proteins.

Chapter 3 Functionalization of the Electrode Surface

3.1 Introduction

The human brain is comprised of hundreds of billions of nerve cells that are connected to form a network. This network is responsible for advanced functions as information is passed through junctions called synapses. The formation of these neural networks is not a result of chance, but rather is created by the interaction between the axon's presynaptic terminal and the postsynaptic dendrite terminals. Adhesive molecules responsible for synapse formation and induction are present on the surface of the branches of neurons and are collectively referred to as synapse organizers. Approximately ten types of membrane molecules have been identified as synapse organizers[41][42][43]. Synapse formation has a selection-specific property because the formation of a synapse occurs after the axon terminal is induced to the target neuron and often travels long distances to specific target areas.

Representative synapse organizers of axon terminals include Neuroligin (NLGN), Semaphorin, and receptor-type protein tyrosine phosphatases (RPTP)[42][44][45]. These synapse organizers drive axon terminals to grow into target cells, but the mechanism for recognizing synapse organizers present in target cells has not yet been fully understood [46]. The first reported synapse organizer was NLGN, but much more is known about RPTP in terms of its substrate specificity, biological function, and role in human disease [47]. RPTPs are a large protein family with 8 subtypes based on different extracellular domains, including common leukocyte antigen-related (LAR), PTPσ, and PTPδ, which have 66% identical amino acid composition. RPTP exists as a membrane protein,

composed of a membrane-proximal D1 domain and a membrane-distal D2 domain with strong catalytic activity toward the interior of the cell. The extracellular portion of RPTP contains immunoglobulin-like (Ig) and fibronectin III (FNIII) domains, which are typically used for cell adhesion (Fig.25). Therefore, cell-specific interactions and directed binding with target cells are possible since neurons have these synapse organizers [41][42][45][48][49].

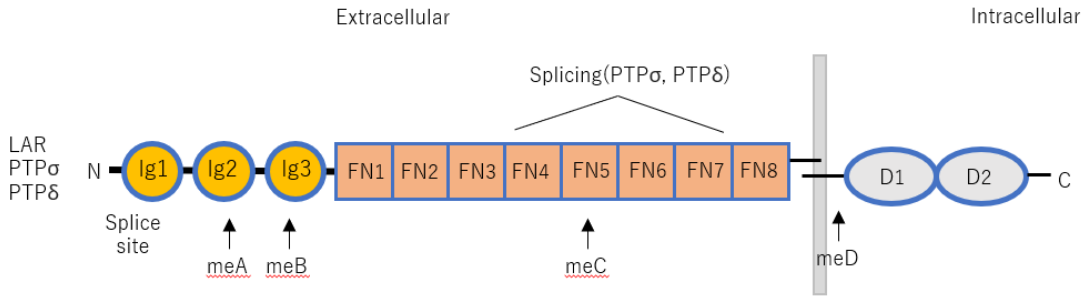

Fig.25 RPTP-type proteins Domains

Initial studies on synapse organizers focused on the growth guidance and regeneration of axons in the central nervous system (CNS). However, in recent years, investigations on the interaction between the presynaptic and postsynaptic have also been actively carried out[41][45][50].

Postsynaptic synapse organizers that interact with presynaptic synapse organizers include NRXNs and tyrosine phosphatase type 2A (2A type RPTPs). These two proteins are present in the postsynaptic dendrites and are called synapse organizers. NRXNs interact with Neuroligins (NLGNs), and type 2A RPTPs interact with receptor-type protein tyrosine phosphatases (RPTPs). Types of 2A type RPTPs include TrkC, Interleukin-1

receptor accessory protein (IL-1RAcP), Interleukin-1 receptor accessory protein-like-1 (IL1RAPL1), and Slitrks [41][42][45].

In this study, I used the IL1RAPL1 protein type. The extracellular domain (ECD) of IL1RAPL1 is present in all vertebrates and is involved in presynaptic differentiation and induction. It has been reported that IL1RAPL1 selectively interacts with the Ig-like domains of PTPδ [51]. There is a total of six known IL1RAPL1 types: R1/, R2A, R3, R4, R5, R6, R7, and R8. R1/6 has a single fibronectin type III domain (FNIII) and two cytoplasmic phosphatase domains in its extracellular region. Type R2A has three NH2-terminal immunoglobulin-like (Ig) domains and nine FNIII domains. R3 has 15 FNIII domains and only one cytoplasmic phosphatase domain. R4 has very short, often glycosylated, extracellular domains, while R5 has a single FNIII domain. R7 and R8 have only one cytoplasmic phosphatase domain, with R7 having a short extracellular domain and R8 having an RDGS (Arg-Gly-Asp-Ser) adhesion recognition molecule [52].

In this experiment, the interaction between electrodes and cells was observed using PTPδ and Fc. To provide cell-specific selectivity induction on the electrode surface, R8, an interleukin receptor accessory protein, was attached to the electrode.

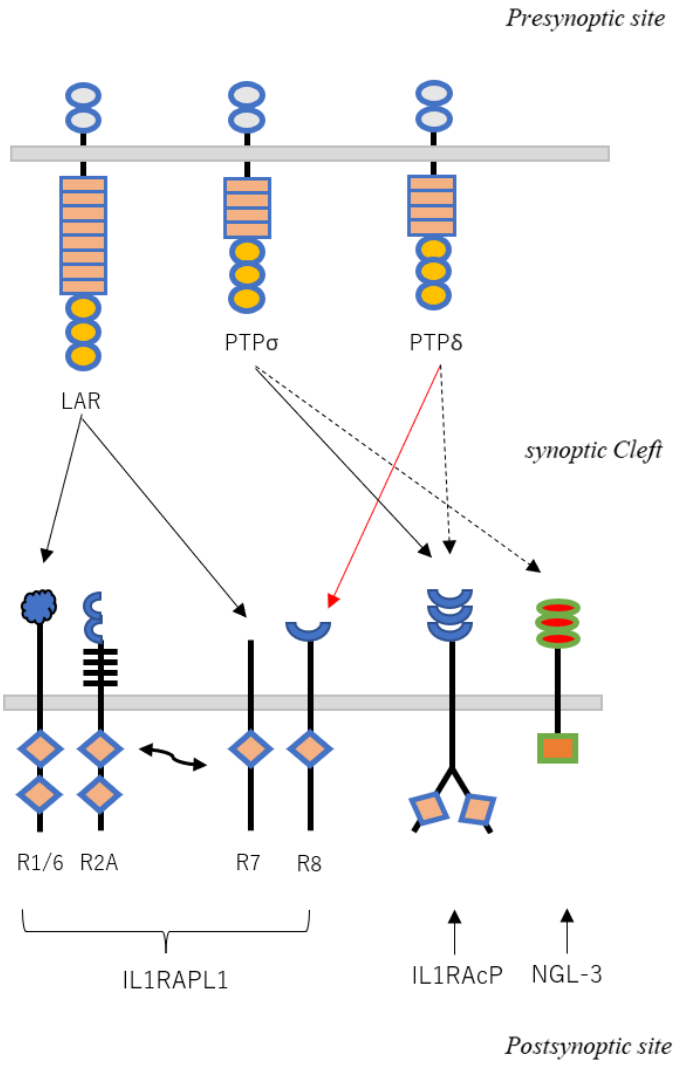

Fig.26. IL1RAPL1 type protein Domain

3.2 Materials and Methods

3.2.1. Protein Extraction

The protein extraction process was carried out as follows: transformation, DAN extraction, transfection, and protein harvesting. It is important to exercise caution during the biochemical work, as contamination is prone to occur.

1. Transformation

The plasmid of the synapse organizers used in this study was obtained from Toshiyuki Yoshida (professor) of Toyama University. A transformation was performed to increase the amount of DNA using the DH5α (E. coli) bacterium. The transformation was achieved by heat shocking the DH5α cells with the DNA, followed by incubation and spreading of the transformed cells on an LB plate (Amp) and culturing in an incubator. The cells were then harvested, and the DNA was extracted using the Midi Kit (U0410B MACHERE-NAGEL).

2. DNA extraction

The procedure of the DNA extraction is detailed below:

- The LB medium containing the cultured cells was centrifuged at 7000 rpm for 5 minutes, leaving only the sediment.
- The RES, LYS, and NEU buffers were added to the sediment, followed by centrifugation at 10,000 rpm for 5 minutes. The supernatant was transferred to a column and washed with the wash buffer.
- The DNA was eluted from the column by adding the Elution buffer and IPA, followed by centrifugation at 15,000 rpm for 30 minutes. The supernatant was then discarded, and the DNA was extracted by adding 70% EtOH and centrifuging at 15,000 rpm for 10 minutes.
- The amount of DNA was measured using a spectrophotometer.

2. Transformation

The transfection method used in this study was the chemical method by PEI. The transfection was performed on HEK 293 cells. The procedure of the transfection is described below:

- The HEK cells were prepared and the DNA, PEI, and DMEM were added to a 1.5ml tube.
- The mixture was left at room temperature for 15-20 minutes.
- The solution containing the DNA was added to a dish containing the HEK cells and gently shaken.
- The dish was then cultivated in a 37℃, 5% CO2 incubator overnight.
- After 3 to 4 days, the culture medium (DMEM_2% FBS) was added to the dish, after After disposal of the existing culture medium (DMEM_10% FBS).
- The culture medium was harvested and used for further experiments.

3.2.2 Measurement of Harvested Protein Quantity

The harvested proteins in this experiment were Venus and R8, which have Fc domains, and PTPδ, which has Venus as a fluorescent factor. The quantity of each protein was measured before use. For the fluorescent proteins Fc-Venus or PTPδ-Venus, their quantity was measured using Jasco's spectrofluorometer Fp8600. In the case of Fc-R8, which is not a fluorescent protein, its quantity and condition were measured using the Dot Blotting method and the ProteinA bead method.

1. Binding Stability assay of Fc-R8 and PTPδVenus

The binding stability of Fc-R8 and PTPδVenus is assessed using the protein A beads test technique. Protein A beads were immersed in DMEM (2% FBS) and five different Fc-R8 solutions (2ng/µl, 4 ng/µl,8 ng/µl,16 ng/µl,32 ng/µl), with varying concentrations. Finally, fluorescent observe with an optical microscope whether Venus is attached to the surface of Protein A beads after taking out Protein A beads from the PTPδVenus solution. Finally, the presence of Venus attached to the surface of Protein A beads is observed using an optical microscope after taking out Protein A beads from the PTPδVenus solution.

2. Dot Blotting Method

Dot blotting is a technique used to detect proteins in molecular biology experiments. It is performed by single-point spotting on a PVDF membrane.

In the Dot Blotting method for measuring the quantity and condition of Fc-R8, which does not have fluorescence, the following procedure was performed:

- Five test samples were prepared by diluting Fc-R8 (2ng/µl, 4 ng/µl,8 ng/µl,16 ng/µl,32 ng/µl).
- Short PVDF membranes were prepared and soaked in methanol.
- The membranes were immersed in deionized water for 10 minutes and then in Blotting Buffer for 5 minutes.
- Blotting the prepared five Fc-R8 samples, DMEM (2% FBS), and freshly harvested Fc-R8 onto the PVDF membrane.

- The PVDF membrane is immersed in a solution of 5% Skim-Milk/TBST for 1 hour at room temperature.
- It is then immersed in a solution of HRP-Conjugate anti-human-Fc antibody and 5% Skim-Milk/TBST for 1 hour.
- The PVDF membrane is washed with TBST for 5 minutes, 3 times.
- The color change is observed while drying.

Component ratio of Blotting Buffer
25mM Tris pH8.3
192mM Glycine
20%v/v methanol

Component ratio of 5%Skim-Milk/TBST
50mM Tris
138mM NaCl
2.7mM KCl
0.1% Tween
pH 7.4

Table.3. Component ratio of "Blotting Buffer" and "5% Skim-Milk/TBST"

3.2.3. Functionalization of Electrodes

In order to impart inductive properties to the electrode, the Fc-R8 protein can be utilized, but it lacks a direct binding site to the solid surface of the electrode. Hence, it is imperative to attach a protein capable of binding to the gold surface of the electrode before conducting the main experiment. The linking factor employed for this purpose is proteinA.

1. Protein A

ProteinA is present in the cell wall of Staphylococcus aureus (Staphylococcus aureus). ProteinA specifically binds to the Fc region of immunoglobulins (mainly IgG). With four affinity binding sites for IgG, it can selectively bind to proteins with an Fc domain and is known for being able to be adsorbed on the surface of gold. In addition, activity can be maintained even after exposure to denaturants such as 4M Urea or 6M Guanidinium chloride. Like this, Protein A has a strong ability to maintain activity. For these reasons, we adopted Protein A.

To prepare the Protein A solution, dilute it with 20 mM Hepes 9.0 pH so that its concentration (10 mg/mL) becomes 0.1 mg/mL. Then, add 5 mM NaCl. The prepared solution is then added to the electrode bath (Fig. 14). A voltage is applied using a SMU device, as specified in Table 1, which is in the form of a pulse. A total of 100 to 200 times at 100 pulses at 50ms intervals were applied. After the voltage application is complete, remove the solution and wash it with MilliQ. Finally, add the Fc-Venus solution to the electrode bath and incubate it in a 5℃ incubator. The Fc-Venus is used to confirm the

adsorption of Protein A on the electrode surface.

2. Cross-link between Fc-R8 and Protein A

After confirming the presence of ProteinA using Fc-Venus, the Fc-Venus was removed using 4MgCl2. Then, Fc-R8 was added to the electrode bath. To form a cross-link between Fc-R8 and Protein A, DSS and DMSO were used. Cross-linking is a technology that strengthens the bond between polymers by altering their physical and chemical properties through various chemical means. In this experiment, DSS (disuccinimidyl suberate) and the organic solvent DMSO (Dimethyl sulfoxide) were used for cross-linking. DSS is an amine-specific protein cross-linker with NHS-ester reactive groups, making it suitable for conjugation with primary amines [53][54]. As DSS is not water-soluble, it must be dissolved in an organic solvent such as DMSO or DMF [53]. With no toxic by-products, DSS is widely used in protein cross-linking experiments. Some proteins, such as Protein A or G, which have an antibody binding site, generally have lysine (K) residues and several primary amines at the amino terminus of the polypeptide. Therefore, DSS reacts with the primary amine of Protein A to form an amide bond. The process of amide bond formation is illustrated in Fig 27.

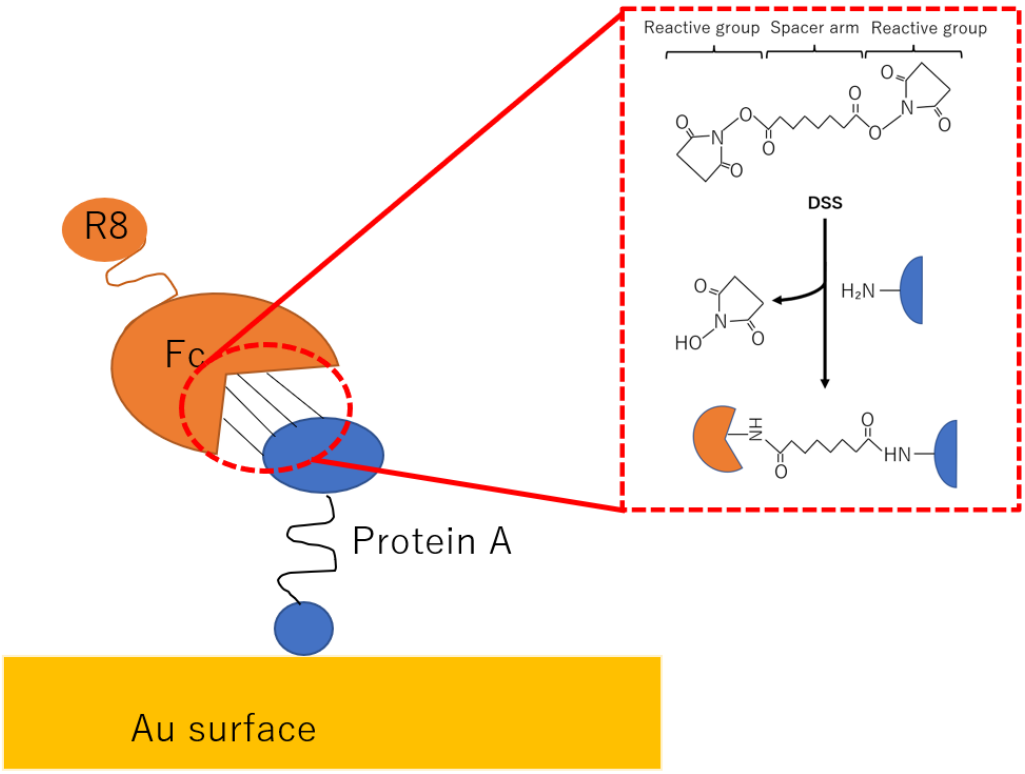

Fig.27. Indicates the formation of an amide bond between two proteins through a DSS reaction. The spacer arm of DSS forms an amide bond between the amide groups of the two proteins.

In this experiment, a 0.5 mM DSS solution was prepared by diluting DSS to 1 M DMSO and then using PBS. Then, add 0.5 mM DSS solution to the electrode bath and incubate for approximately 10 minutes. Finally, the presence of Fc-R8 on the electrode is confirmed using PTPδVenus.

3. Investigation of Protein Binding Credibility

We investigated the correct binding of proteins in each component by using several proteins. To confirm the binding of Protein A, we used Fc-Venus with a Fc domain.

Additionally, to assess the function and accuracy of binding of R8, we utilized Fc-Mcherry with a Fc domain and PTPδVenus with a PTPδ domain. Fc-Venus and Fc-Mcherry are fluorescent proteins with Fc domains created through transformation. Venus (Ex λ: 515, Em λ: 528) emits yellow fluorescence, while Mcherry (Ex λ: 587, Em λ: 610) emits red fluorescence.

PTPδ is a class of receptor-type protein tyrosine phosphatases (RPTPs) and is induced by IL1RAPL1, selectively binding with IL1RAPL1.

4. Density Estimation of Fc-R8 on Electrode Surface

To estimate the density of Fc-R8 on the electrode surface, a circular chamber of approximately 20μm in diameter and 5μm in height (volume of the su8 chamber: 15.7 x 10^-6μL) was fabricated on an Au/Cr substrate using su8-3005. Fc-R8 was attached to the Au surface inside the su8 chamber through a similar process as the functionalization of the electrode. To visualize Fc-R8, PTPδVenus (concentration 2.8μg/μL) was added and incubated for approximately 8 hours in a refrigerator at 5°C. The quantity of Fc-R8 can be estimated from the quantity of PTPδVenus observed because the Fc-R8 domain interacts one-by-one with the PTPδ domain. The fluorescence of Venus was observed using an optical microscope, and the fluorescence information observed on the Au surface inside the su8 chamber is a standard for the protein quantity per area.

5. Formation of Synapses between Electrodes and Neurons with R8

Initially, wash the electrode that has been attached with FcR8 with PBS and place the neuron cells into the electrode bath with the culture medium. Incubate the neurons in a CO2 incubator for 5 days. Finally, label the site of synaptic formation with SVP-38(anti-Synaptophysin antibody) and confirm it through optical microscopy to observe the formation of synapses.

3.3 Result

3.3.1. Protein Extraction and Analysis

The protein extraction process includes Transformation, DNA extraction, transfection, and finally, Protein Harvest. Fc-Venus, Fc-R8, and PTPδ-Venus were obtained through this process. Fig 28 illustrates the complete procedure of protein extraction.

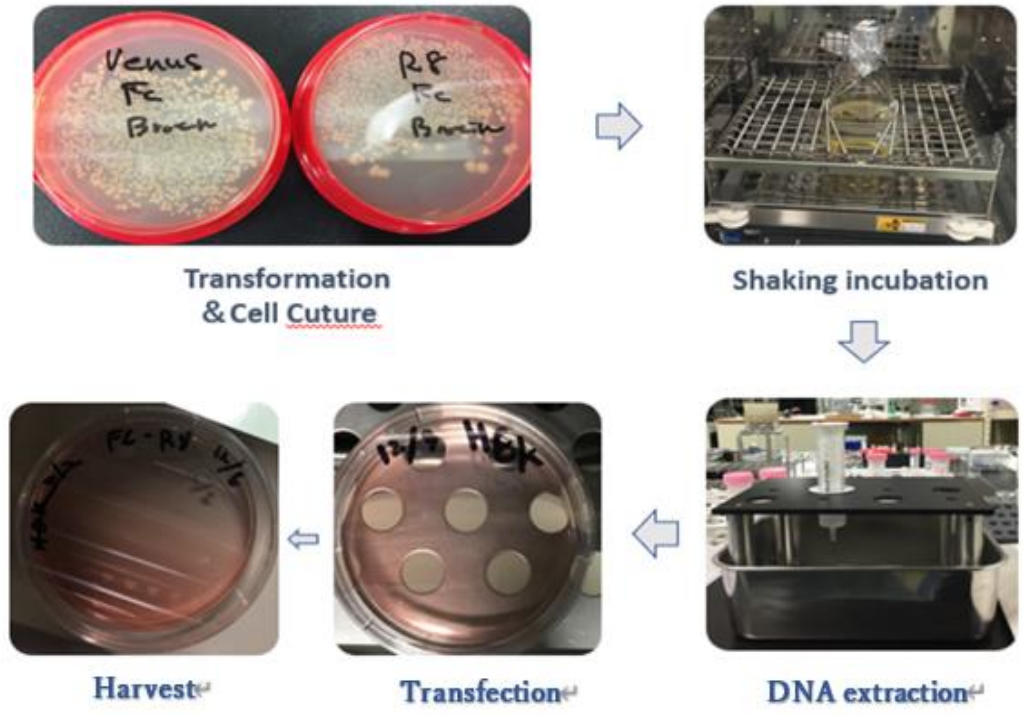

Fig.28. (A) DH5α (E. coli) was cultured in Plate LB medium (containing ampicillin) after transformation. (B) The process of isolating a single colony from Plate LB. (C) DNA was extracted using the Midi Kit U0410B. (D) The transfection process. (E) The protein was harvested after a 5-day culture period.

Fig 29 shows the changes in the state after transfection at about 1-day intervals. an increase in fluorescent protein after transfection was observed through a microscope.

Fig 30 shows that fluorescence values of the fluorescent proteins of Fc-Venus and PTPδ-

Venus were measured with a spectrofluorometer.

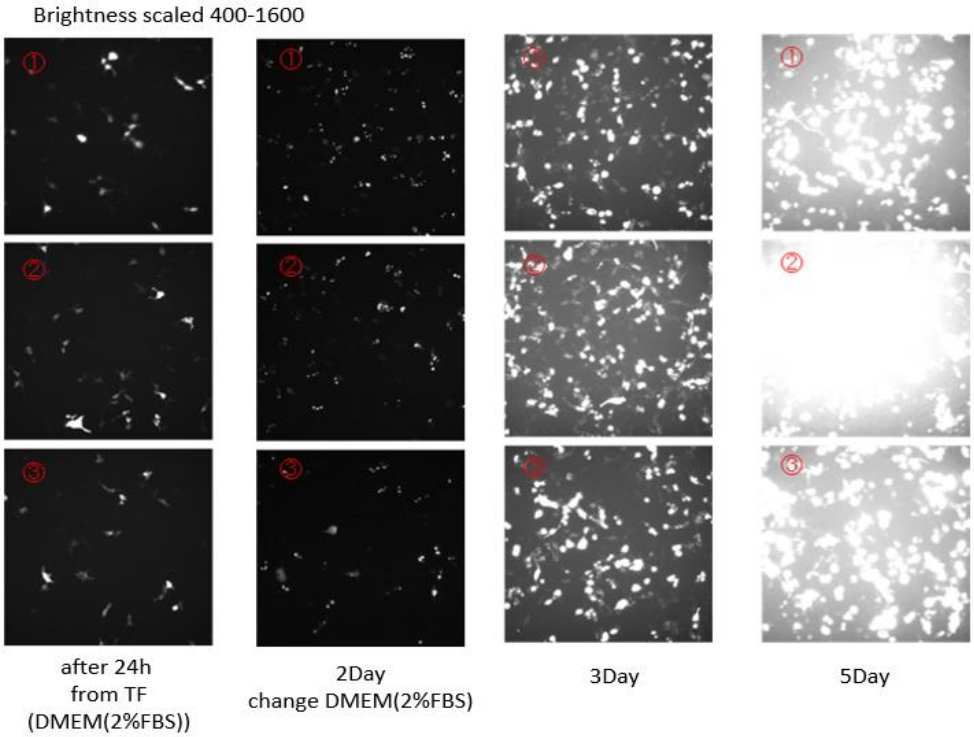

Fig29. This is the result of observing the growth process of PTPδ-Venus. On each day, three areas were randomly selected and observed. After 24 hours from the transfection, the culture solution was replaced with DMEM (2% FBS). Fc-Venus underwent the same process.

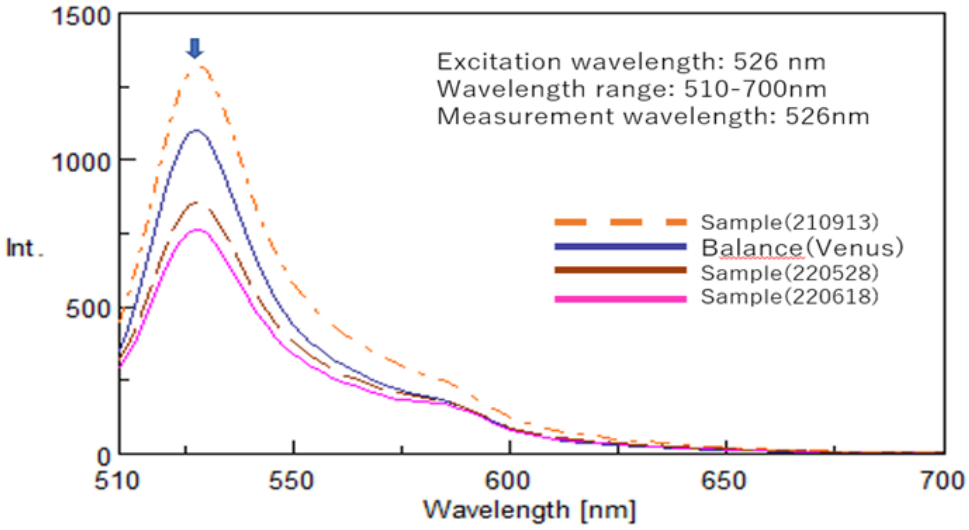

Fig.30. The result of observing the sample of Venus with a spectrofluorometer.

After harvesting FcVenus and PTPδ-Venus, the fluorescence values were measured using a spectrofluorometer. Fig.30 shows the measured fluorescence intensity of the Venus-tagged proteins. The fluorescence intensity varied depending on the type of DNA and the state of Hek cells. Therefore, this experiment only used proteins with fluorescence intensity above the baseline. The quality of the harvested protein was monitored and maintained through the process shown in Fig.30.

3.3.2. Verifying the Binding Stability between Fc-R8 and PTPδVenus using ProteinA-beads

The stability of the binding between Fc-R8 and PTPδ-Venus was assessed by using ProteinA-beads.

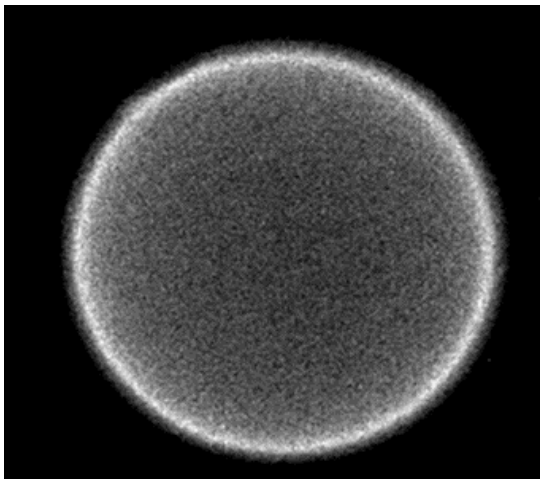

Fig.31. This results from testing the stability of the combination of Fc-R8 and PTPδVenus using ProteinA-beads.

This Fig.31 demonstrates that the Fc domain and R8 domain of Fc-R8 were expressed as expected. Additionally, this result shows that the PTPδ domain of PTPδVenus was also

successfully expressed. Based on these results, it can be concluded that the harvested protein did not have any significant issues.

3.3.3. Examination of Fc-R8 by Dot Blotting

The amount of harvested Fc-R8 per microliter was confirmed through dot blotting. Table 4 shows that the protein concentration is approximately 1ng/µl.

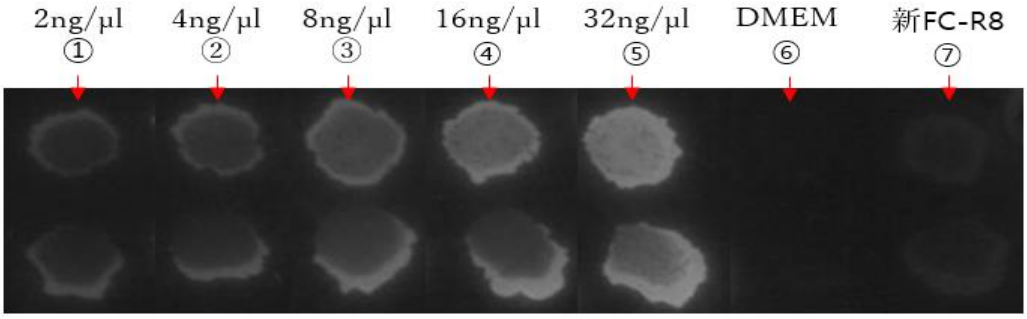

Fig.32. It shows the concentration of Fc-R8 spotted on the PVDF membrane. The brighter the image, the higher the concentration of Fc-R8, indicating an increased binding with PTPδVenus.

Concentration of Fc-R8	The mean value of fluorescence intensity
0 ng/µl（DMEM）	24.812 A.U
2ng/µl	41.212 A.U
4 ng/µl	50.338 A.U
8 ng/µl	66.927 A.U
16 ng/µl	83.732 A.U
32 ng/µl	101.13 A.U
新FC-R8	34.935 A.U

Table 4. It indicates the fluorescence intensity values obtained from measuring the brightness of PTPδVenus, which was bound to Fc-R8 present on the PVDF membrane. The fluorescence intensity was measured using HCImageLive.

The fluorescence intensity of each sample was measured using HCImageLive and recorded in Table 4

3.3.4. Investigating the Effectiveness of Protein Binding

The objective of this experiment was to use a synapse organizer, IL1RAPL1, to give the electrode the ability to induce synapse formation in neurons. However, the synapse organizer cannot directly bind to the solid surface of the electrode. To overcome this, ProteinA was used as an intermediate bridge. Therefore, the binding of the proteins was confirmed step by step. The fabrication of the electrodes followed the procedure outlined in Chapter 2.

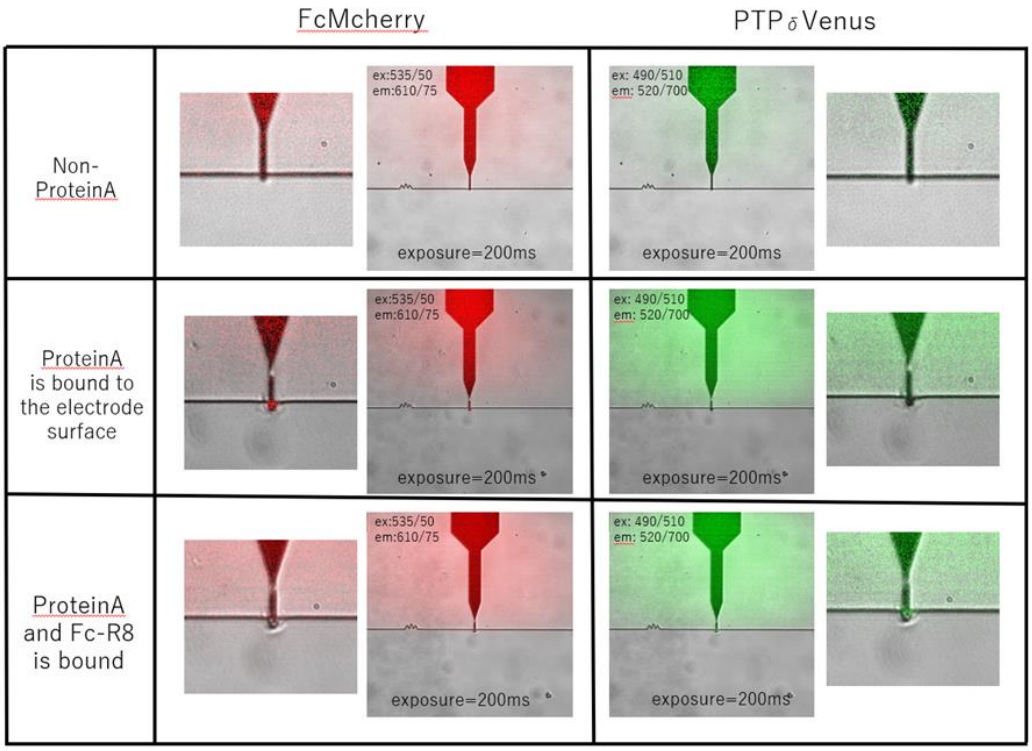

Fig 33. It depicts the stepwise binding of proteins. Figures A and B show that ProteinA selectively binds to the Fc domain through FcMcherry. Additionally, the data in Figures B and C demonstrate that the R8 domain selectively binds to PTPδVenus.

Fig.33 shows that my experiment achieved its goal through the stepwise binding of proteins. When protein A was absent, FcMcherry and PTPδVenus were not observed on the electrode surface. However, when protein A was present, FcMcherry was observed on the electrode surface, but PTPδVenus was not. This indicates that protein A is present on the electrode surface and can only bind to proteins with the Fc domain. On the other hand, only PTPδVenus was observed on the electrode surface where protein A and Fc-R8 were bound. This suggests that R8 only interacts with the PTPδ domain. However, FcMcherry was not observed on the electrode surface where Fc-R8 was present, because Fc-R8 was already bound to protein A and interfered with FcMcherry binding.

3.3.5. Observation of IL1RAPL1 Adsorbed on the Electrode Surface

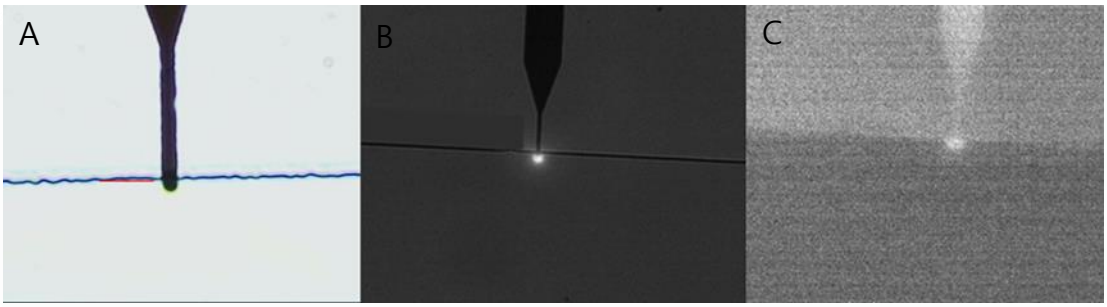

Fig. 34 A) The result of observing the state of the electrode using an optical microscope. B) The confirmation result of protein A adsorption through the use of Fc-Venus. C) The results demonstrate the combination of Fc-R8 and PTPδVenus on the same electrode, with the binding between the two proteins, lasting for more than five days.

Fig. 34-A shows the result of observing the electrode under 40x magnification using an optical microscope. The bottom is the electrode, while the top is coated with photoresist.

To functionalize the electrode, i attached Protein A to its surface. I used FcVenus to confirm the presence of protein A, as protein A is invisible to the naked eye. Protein A can specifically bind to the Fc domain of immunoglobulins, mainly IgG. Fig. 34-B shows that FcVenus was observed on the electrode surface after binding protein A to it, proving that protein A has bonded to the electrode. Next, 4M MgCl2 was used to break the bond between protein A and FcVenus, and then PTPδVenus was added.

Fig. 34-C shows the results after 5 days of cross-linking between Fc-R8 and Protein A. This result indicates that Protein A, Fc-R8, and PTPδVenus were bound in order on the electrode surface as a result of the experiment process. Additionally, Fig. 34-C shows that the binding can be sustained for a long time due to the cross-linking applied.

3.3.6. Quantification of Adsorbed IL1RAPL1 on the Electrode Surface

In this investigation, i evaluated the concentration of IL1RAPL1 (R8) present on the electrode surface. To do this, i used purified PTPδVenus (concentration 2.8 µg/ul) as a reference. The R8 domain and PTPδ domain of the protein form a 1:1 bond, which made this calculation possible. The molecular weight of PTPδVenus was 125 kDa, and the calculation was performed after converting the molecular weight to molarity (125 x 10^3 g/mol). The concentration of purified PTPδVenus solution (2.8 µg/ul) was divided by the molecular weight of PTPδVenus (using Avogadro's constant: 6.022 x 10^23). This calculation showed that the concentration of PTPδVenus was 1.35 x 10^13 protein/µl.

Fig.35. A depicts a su8 chamber with a volume of approximately 1.57 x 10^-6 ul. It contains approximately 2.12 x 10^5 proteins/well of PTPδVenus. The average surface area of each electrode, shown in B, C, and D, is approximately 4.5 um².

I diluted the purified PTPδVenus solution 1/100 with a buffer solution to create a solution for the experiment. Fig. 35-A shows that a solution containing 1.35 x 10^11proteins/ul was successfully stored in the chamber, with a volume of about 15.7 x 10^-6ul. We measured the fluorescence intensity of the PTPδVenus confined in the SU8 chamber using HCImageLive. The microscope light intensity was approximately 1.565mW. The observed fluorescence intensity of PTPδVenus in the chamber was 55947.612. I calculated the protein value by dividing the volume of the protein in the SU8 chamber by the volume of the chamber. i obtained a result of 2.12 x 10^5proteins per well. Based on this value, I investigated the protein value of each electrode, which has a surface area of 4.5μm².

I found that the protein value on each electrode was B: 2.888 x 10^4 protein/μm², C: 2.2444 x 10^4 protein/μm², and D: 1.3088 x 10^4 protein/μm². On average, protein was present on the electrode surface at a level of 2.147 x 10^4 protein/μm², with a standard deviation of 0.631 x 10^4 protein/μm².

In the synapse observation experiment, a larger-sized electrode was used to facilitate the

observation of synapses. However, after the experiment, the electrode size was significantly reduced to enable a 1:1 coupling between the neuron cell and the electrode. The previous electrode was about 100 times larger than the current electrode size.

3.3.7. Observation of Synapse Formation between Electrodes and Neurons

Fig.36 demonstrates that the PTPδ domain at the axon terminals of neurons interacted with the R8 domain on the electrode, leading to the formation of synapses between the axon terminals and R8 domain. In the figure, the red dots represent the synapses stained by SVP-38 (anti-Synaptophysin antibody).

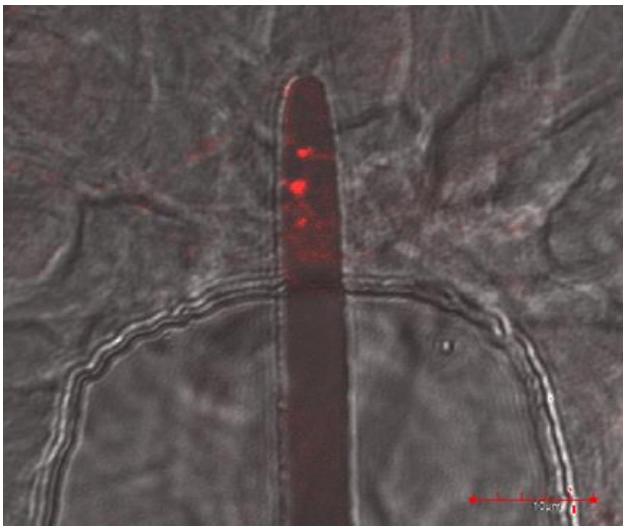

Fig.36. The red stain in Fig.36 indicates the presence of these formed synapses between the axon terminals of neurons and the R8 domain on the electrode.

The axon terminals possess the PTPδ domain, which extends towards the electrode with R8 domain, resulting in the formation of a synapse through their interaction. Hence, this result indicates that the neuron cell recognizes Fc-R8 on the electrode surface.

These results indicate that it is possible to investigate binding properties based on cell

type characteristics in relation to electrodes.

3.4 Discussion

3.4.1 Evaluation of Protein

The proteins used in the experiment were harvested in a consistent manner and used after verifying their functionality. Fig.31 shows that both Fc-R8 and PTPδVenus have functional binding domains. However, harvesting high-quality Fc-R8 proved to be challenging. Table 4 shows that the amount of harvested Fc-R8 is low. However, it was difficult to make precise measurements due to the high brightness of the PVDF membrane.

3.4.2 Evaluation of protein functionalization step by step

Fig 33 highlights the significance of sequential binding. In the case of electrodes without protein A, as shown in Fig 33, nothing was observed. This result suggests that FcMcherry and PTPδVenus cannot exist in areas without protein A. Additionally, FcMcherry was observed in electrodes where only protein A was present. This indicates that a protein with an Fc domain can only be present in areas where protein A is present. Only PTPδ-Venus was observed in areas where protein A and Fc-R8 are assumed to be binding. However, FcMcherry was not observed anywhere. This result implies that PTPδ-Venus can be present in areas where R8 is present. The absence of FcMcherry in areas where protein A and Fc-R8 are assumed to be binding may be due to Fc-R8 occupying the binding site.

3.4.3 Observation of IL1RAPL1 Adsorbed on the Electrode Surface

Fig 34 shows that Protein A and Fc-R8 form an amide bond through cross-linking. However, when the cross-link treatment was not performed, desorption of Fc-R8 was observed after 2 to 3 days. This result indicates the high stability of the amide bond. However, the success rate of bonding between protein A and the electrode surface was not always consistent. Further research in Chapter 2 is necessary to address this issue. Additionally, when protein A was adsorbed to the electrode surface, a pulse voltage of 50 ms was used instead of 25 ms. The reason for this is that the electrode broke when a pulse voltage of 25 ms was applied. By settling on the safest experimental method, the success rate of the results in Fig 34-C was increased.

3.4.4 Adsorption of IL1RAPL1 on the Electrode Surface

I confirmed that the synapse organizers known as R8 were present on the electrode surface in an amount of approximately 21470. This result indicates a density of 4771 per electrode surface area (Table.5). Although the amount of IL1RAPL1 present in the active zones of synapses has not yet been identified, previous research has reported a density of synapse organizers at the active zones of synapses ranging from approximately 200 to 400 per square micrometer [54][55]. My results suggest that the synapse organizers of R8 present on the electrodes have a higher density than the density of synapse organizers at the active zones of synapses, indicating that the electrode has the same or greater potential for inducing neurons as the active zones of synapses. Additionally, I confirmed stable synapse

formation between the electrode and neuron through Fig.36. These results indicate no problems with neuron induction and synapse formation.

However, there are still many limitations for practical use. Thus, my next goal is to address these limitations. My new technology for recording action potentials will enable more stable and long-term recording than conventional technologies. It is suggested that this new technology will have applications not only in the field of electrophysiology, but also in neurophysiology and even the medical field.

	well area	well intensity intensity	background intensity		total intensity
PBS	812	408.252	409.683		1.37028E-11
Protein in Chamber	812	539	471.53		55947.612
electorodeB	678	456.847	424.5587		21891.4674
electorodeC	562	451.527	421.0803		17111.0454
electorodeD	350	454.609	426.217		9937.2
Power ratio = 1.565mW					
Protein number ratio = total intensity of electorode/55947x1.565					
Protein/elecotode= 2.12x10^5 x Protein number ratio					

Table.5. The fluorescence intensity of each electrode surface and su8 chamber. The power ratio is 1.56mW.

Chapter 4

Electrical coupling across the neuron-microelectrode junction: numerical simulation study

4.1 Introduction

Recording the electrical activity of neurons is crucial in advancing our understanding of the nervous system [56][57][58][59][60][61][62]. Currently, there are two main approaches to nerve cell recording: the extracellular approach and the intracellular approach. Intracellular approaches mainly use non-invasive electrodes to obtain information from outside the cell, while extracellular approaches using microelectrode arrays (MEAs) have multi-unit electrical recordings with high spatial and temporal resolution [63][64]. However, extracellular approaches have limitations in terms of low selectivity and sensitivity [62][65][66][67]. To overcome these limitations, invasive electrode and clamp techniques have been developed, but they also have drawbacks such as limited duration of use, cell death, and low selectivity [62][66][67].

Recently, fluorescent probe technology with high selectivity and sensitivity has emerged, but it also has limitations in terms of low spatiotemporal and temporal resolution [60][61][66][67]. Therefore, when conducting experiments to record the electrical activity of neurons, researchers use the optimal recording technology that suits the purpose and conditions [25][66][67][68][69]. A recent trend in neuroscience is to perform long-term recording and selective coupling to identify the physiological or pathological function of neuronal circuits [25][60]. Efforts have also been made to integrate non-invasive extracellular and invasive intracellular recording technologies [25][68]. In this study, we introduced specific selectivity to non-invasive electrodes by incorporating the mechanism of a fluorescent probe. We also fabricated electrodes with a width of 1-2μm

to induce wrapping from neuron cells. My goal is to record the long-term electrical activity of a specific single neuron. However, despite the miniaturization of electrodes into micro-units, the problem of low sensitivity remains unsolved. I speculate that this issue is due to the lack of functional analysis of synapse formation between microelectrodes and nerve cells.

In this chapter, I perform a functional analysis of synapse formation between microelectrodes and neurons using simulation. This experiment has several objectives. The first is to construct a simulation model for the new recording method, as it is estimated that this model can guide future research in the same field. Additionally, through simulation, problems can be quickly identified in the electrode-nerve cell system where the new recording method has been introduced. Finally, actual biological experiments require a significant amount of time and money, and it is estimated that simulation modeling can reduce these costs and time requirements.

4.2 Experiment

4.2.1 Circuit Design

To design the circuit of the coupling structure between the junctional membrane of the neuron cell and the microelectrode device, LTspice17.4 was utilized. The coupling coefficient (CC) was imported as a concept to analyze the data of the junctional structure. The CC was defined as the ratio of the output potential recorded by the microelectrode device and the input voltage.

4.2.2 Simulation of the Neuron-Microelectrode Junction

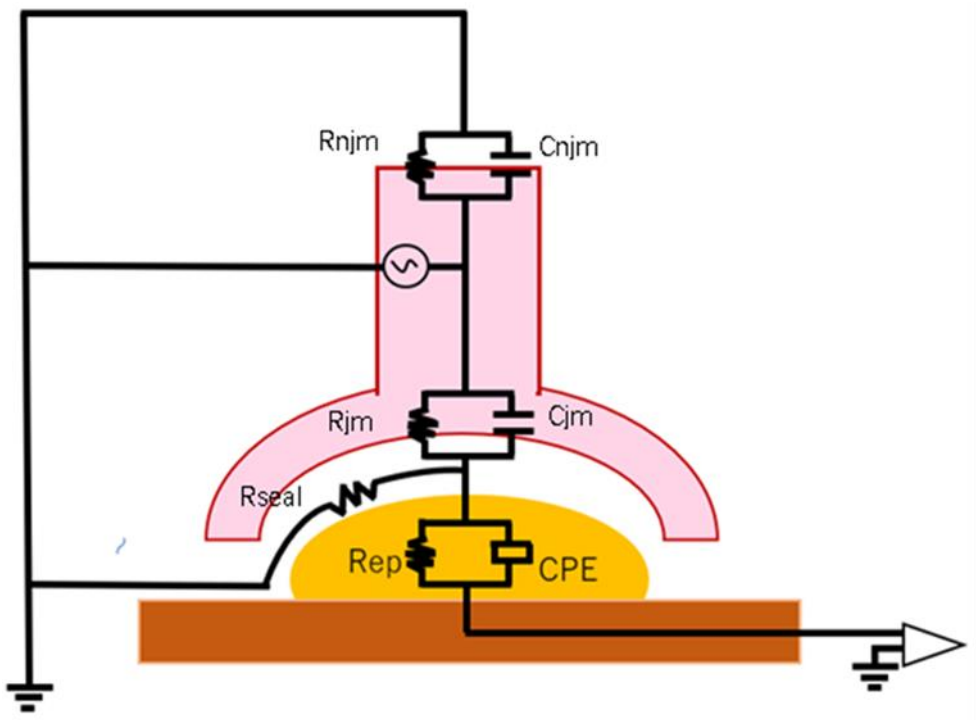

Fig. 37. It shows that neurons are guided to the electrode by the synapse organizer on the electrode surface, resulting in the formation of a coupling with the electrode.

The molecularly induced neuron-microelectrode junction was divided into several parts, including the non-junctional membrane (njm), junctional membrane (jm), and electrode device. A voltage impulse was fed into the cytoplasm to represent the action potentials generated by the cell soma. A seal resistance (Rseal or Rs) was used to represent the cleft between the junctional membrane and electrode surface. To account for noise and insulator leakage in the cell membrane, a leakage current was imported into the circuit. The capacitive current and the resistance current were then summed into two currents.

Each part of the neuron junction circuit was represented by an RC (resistance and capacitance) circuit, with four RC circuits used to represent the non-junctional membrane, junctional membrane, microelectrode, and amplifier [70]. The capacitive current of the membrane capacitance (Cm) was also taken into account. A voltage source was placed between the non-junctional and junctional membranes, representing the synaptic potentials. In this study, two types of voltage sources were used: Vpulse, which was obtained by converting the actual action potential into data, and Vsin, a sin wave used to represent the voltage impulse. In the simulation of the CC, the Vsin was utilized, as it only required the maximal value of the single sine wave and not the details of the voltage wave.

4.2.3 Application of Real Action Potential data

I input the actual action potential data values provided by Professor Tsutsui into the designed circuit. The data values are presented in Fig.38.

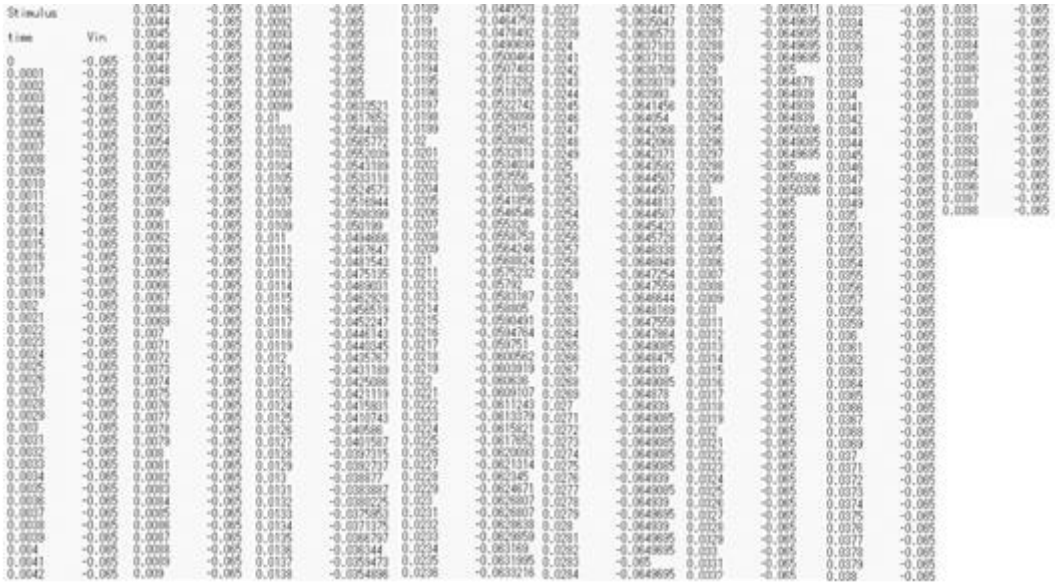

Fig.38. Action potential data

4.3 Result

4.2.1 Circuit diagram of the neuron-electrode junction

In this experiment, I completed the circuit shown in Fig. 39 with the parameters obtained from various sources of literature [25][60][66][71]. The parameters used in the simulation are as follows:

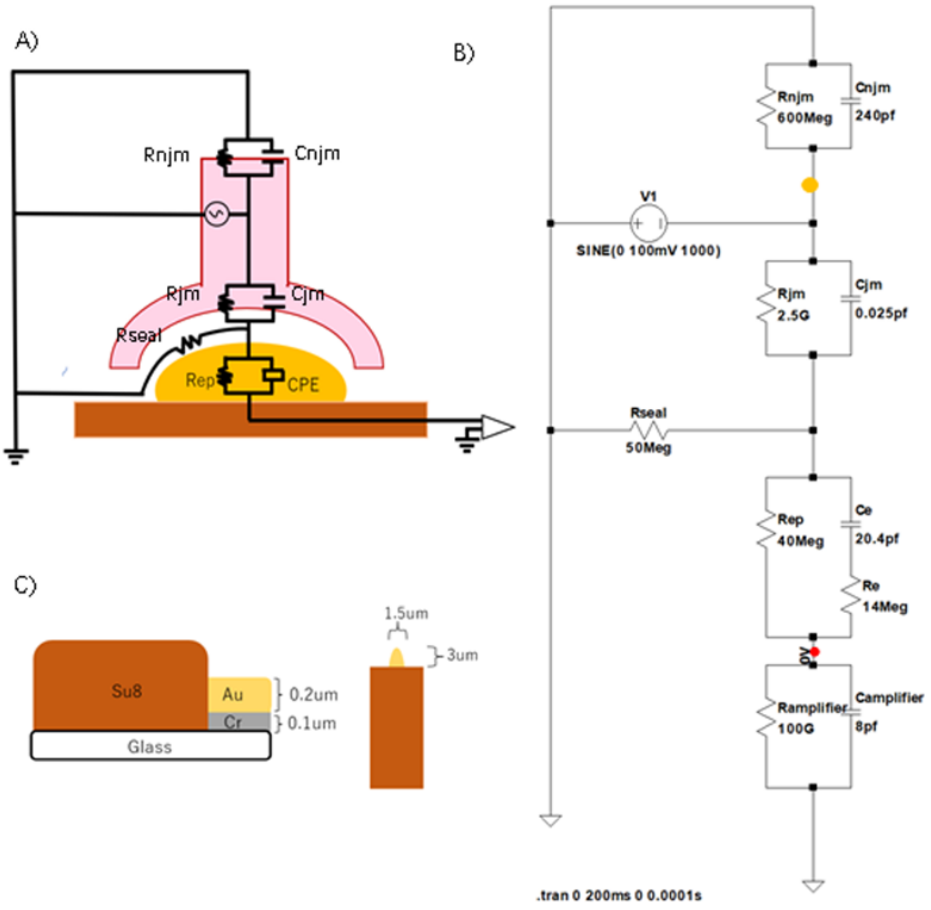

Fig.39. A show the circuit design of the coupling structure between the junction membrane of the neuron cell and the microelectrode device. B represents the structure of the electrode. C illustrates the simulated representation of the coupling between the junction membrane of the nerve cell and the microelectrode device using the data from A and B. The yellow dot signifies the section where the potential is input, and the red dot signifies the section where the potential is output.

The non-junctional membrane capacitance (Cnjm) was set to 200pf, and the range of non-junctional membrane resistance (Rnjm) was selected from 200MΩ to 600MΩ, based on references [72][73]. The microelectrode was designed with a height of 0.3um and a diameter of 1.5um, with a total surface area of 2.48um2 [66]. The junctional membrane resistance (Rjm) was calculated by dividing the area of the neuron cell in contact with the electrode and the area of the electrode, and then multiplying the total input resistance (Rin). The result was an Rjm of 2.5GΩ [60][74][75]. The junctional membrane capacitance (Cjm) was calculated by dividing the total membrane capacitance (Cm) by the ratio of the neuron cell's area to the electrode's area, resulting in a Cjm of 0.025 pf.

The seal resistance refers to the tightness of the seal at the junction between the junctional membrane and electrode surface. In this process, only a small amount of electric current can reach the electrode because the cleft is filled with an ionic solution. Under these conditions, a higher seal resistance indicates that more electric current can flow from the junctional membrane to the electrode surface. We set the range of the seal resistance from 50 to 200 MΩ in our simulation and obtained the relationship between the seal resistance and the coupling coefficient (CC) [71][74].

Two modes were chosen for microelectrode simulation: RC circuit and CPE mode. The CPE is a nonlinear circuit element used in real analog systems. An amplifier of 100GΩ and a camplifier of 8pf was used in all simulations of the neuron-electrode junction circuit [72][73][74][75]. The RC circuit with Re and Ce referred to the leakage current of the electrode base stalk, which was exported directly to the NaCl solution[74][75][76]. The

leakage RC circuit was in contrast to the junctional membrane RC circuit, where Re may increase the CC but Ce decreases the CC.

4.2.2 Performance analysis of neural electrode junction circuit

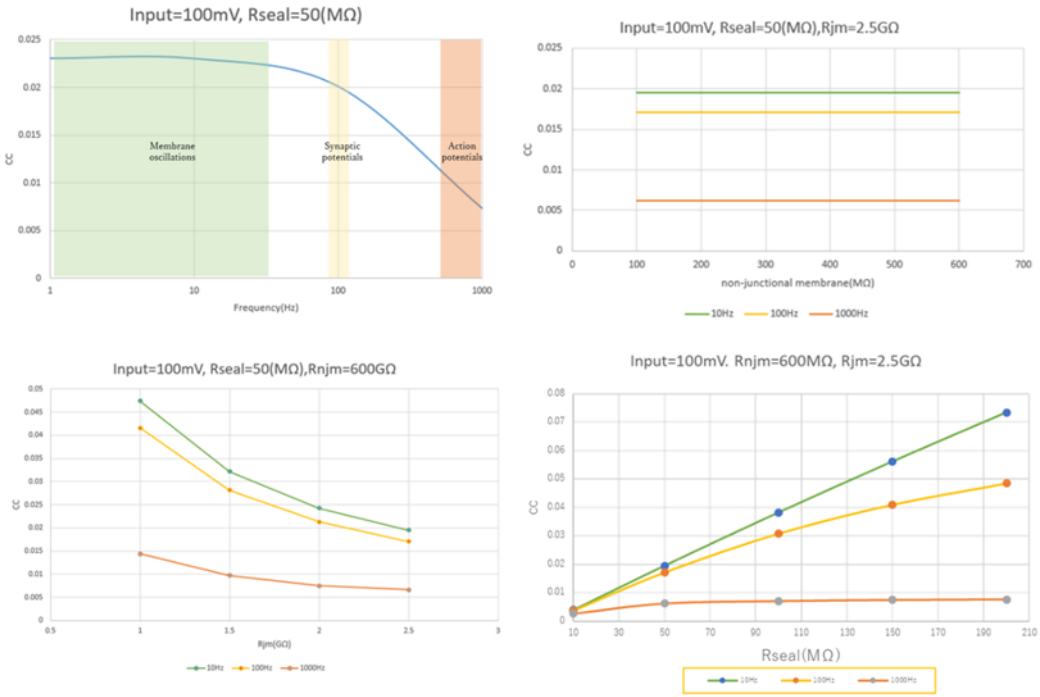

Fig.40. A) Membrane oscillations are represented by the sine wave from 1 to 50Hz. The wave at 100Hz represents synaptic potentials. The range of action potentials primarily lies between 500-1000Hz. B) shows the relationship between CC and Rnjm, where Rjm was calculated based on the input resistance of the axon terminal. C) shows the relationship between CC and Rjm. D) shows the relationship between CC and Rseal. The color of the line represents each frequency.

To determine the relationship between the CC and the frequency of the input voltage, we selected a range of frequencies from 1 to 1000Hz. Fig.40-A depicts the range of the CC as a function of frequency. Membrane oscillations were represented by sine waves from

1 to 50Hz. When a sine wave from 1 to 50Hz was input into the simulation, we obtained a CC range of 0.022 to 0.023. In other words, the CC of the result values obtained when measuring the membrane frequency using our fabricated electrode must fall within the range of 0.022 to 0.023.

A wave of 100Hz represents a synaptic potential. When a sine wave of 100Hz was input into the simulation, we obtained a CC of 0.02. This means that the CC of the result values obtained when measuring the synaptic potential using our fabricated electrode should be equal to 0.02.

Waves between 500 to 1000Hz represent action potentials. When sine waves from 500 to 1000Hz were input into the simulation, we obtained a CC range of 0.013 to 0.008. In other words, it indicates that the CC of the result values obtained when measuring action potentials using our fabricated electrode must be within the range of 0.013 to 0.008.

To determine the relationship between CC and Rnjm, the input resistance of a neuron cell, we selected the range of Rnjm from 100MΩ to 600 MΩ. This range was referenced from various literature sources, as Rnjm increases with distance from the soma [74][77]. Since our experiments focus on action potentials from axon terminals, we set the final Rnjm value to 600MΩ. We then examined the change in CC at each frequency to investigate the relationship between CC and Rnjm. As shown in Fig.40-B, the results indicate that Rnjm has no impact on CC. However, Rnjm has a strong correlation with Rjm, the junctional membrane resistance. Therefore, we also evaluated the relationship between CC and Rjm by varying Rjm while fixing Rnjm(600MΩ) (Fig.40-C).

I calculated the range of junctional membrane resistance (Rjm) using the area data of the junction between the electrode and the neuron cell. The range of Rjm was set from 1GΩ to 2.5GΩ. The non-junctional membrane capacitance (Cnjm) was set at a constant of 0.025 pF considering the calculation of membrane-specific capacitance. Fig.40-C shows that the function between the coupling coefficient (CC) and Rjm has a downward trend, meaning that the CC decreases as Rjm increases. Fig.40-C also shows the CC-frequency function over the range of Rjm. The recordings of membrane oscillations (10Hz), synaptic potentials (100Hz), and action potentials (1000Hz) tend to decrease rapidly as Rjm increases. However, the decline of the function slope width for action potentials (1000Hz) is lower than that of membrane oscillations and synaptic potentials. This result indicates that the output voltage recording becomes very small at the action potential.

In Fig.40-D, I also investigated the relationship between CC and Rseal (Resistance Seal). The range of Rseal was set from 10 MΩ to 200 MΩ. The final value of Rnjm (input resistance) was set at 600 MΩ, considering our experiments examining action potentials from axon terminals. In the simulation, Rjm was set to 2.1 GΩ and Cjm to 0.0025 pf. Rjm was calculated by multiplying the ratio of the area between the neuron cell and the electrode by the input resistance (Rnjm = 600 MΩ), and Cjm was calculated by multiplying the ratio of the gap between the neuron cell and the electrode by the membrane-specific capacitance (0.1 pf). Fig.40-D shows that the value of CC increases as Rseal increases. This result suggests that the recording quality of the output improves as Rseal increases. Additionally, we also confirmed the relationship between frequency

and CC with a variable of Rseal. The CC showed a significant increase at 10 Hz and 100 Hz, but the range of increase gradually reduced at 1000 Hz, indicating poor recording quality at 1000 Hz (action potential).

4.2.2 Virtual Recording of Action Potential

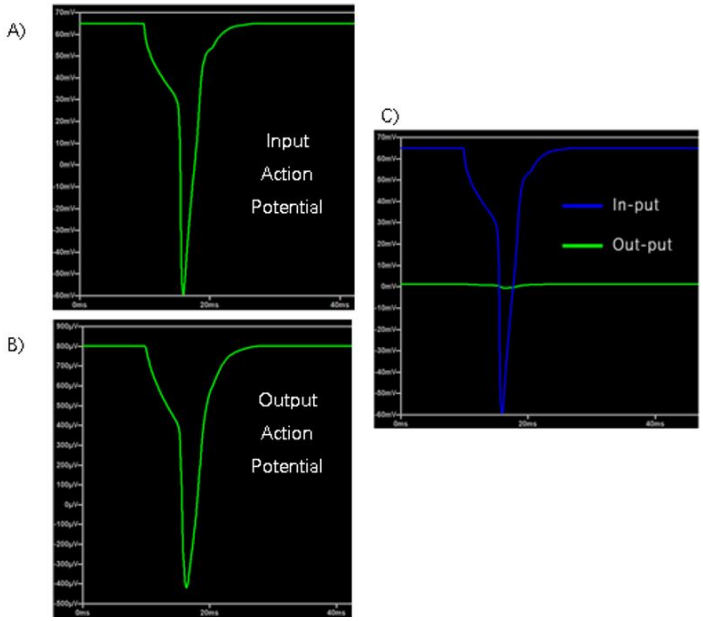

Fig.41. A displays the input voltage, B shows the output voltage, and C presents the value of the recorded output voltage obtained when using the fabricated electrode.

Finally, the simulation was conducted using actual action potential data (Vpulse). The results of inputting the action potential data are shown in Fig 41. As seen in Fig 41-c, the output voltage value was approximately 1.2mV for a total input voltage of 125mV. The coupling coefficient (CC) was calculated by dividing the output voltage value by the input voltage value and was found to be approximately 0.0184. This indicates that only 0.96% of the input voltage was obtained as the output voltage value. The range of the CC-frequency function was from 0.013 to 0.008, which indicates that the result obtained from

inputting the Vpulse was not within the frequency range of the action potential. This suggests that it may be challenging to record action potentials from nerve cells using the fabricated electrodes.

4.4 Discussion

I used simulations to evaluate the performance of new electrophysiology techniques applied to fabricated electrodes. First, I created an analog circuit, as shown in Fig. 39-B. I created the analog circuit by referencing various literature and previous data from my lab [25][66][71][78]. The CPE (constant phase element) circuit was determined by considering factors such as the surface state of the electrode, the OSFET (Oxide-semiconductor Field Effect Transistor), and the state of the electrode in the solution. Thus, we used the CPE to represent the electrode device since the electrode was not a pure impedance. In reality, the CPE, which consists of capacitance and resistance, was sufficient for recording output potentials, and I added a parallel resistor to make the circuit more stable. The CPE value was obtained by comparing the size of electrodes in past literature with those currently in use. Therefore, the CPE parameters were not directly obtained through experiments and may contain errors.

I obtained the input and output voltages from the input and output points in the circuit. Then, I divided the output voltage by the input voltage to obtain the CC. As seen in Fig.40-A, the frequency range of action potentials (1000Hz) has a CC range of approximately 0.013 to 0.008. However, in simulation results using actual action potentials, the CC

values were not found to fall within the range of action potentials.

Fig. 40-B shows the function between CC and Rnjm of the input voltage. In principle, the non-junctional membrane resistance does not affect the movement of electrophysiological signals from the junctional membrane to the electrode surface, as demonstrated in Fig. 40-B.

Fig. 40-C shows the function between CC and Rjm of the input voltage. Looking at the results of Fig. 40-C, reducing Rjm increases the CC value. As the area of the electrode increases, Rjm tends to decrease. However, when the electrode becomes larger, the phenomenon of wrapping the electrode during synapse formation disappears, which means Rseal is excluded.

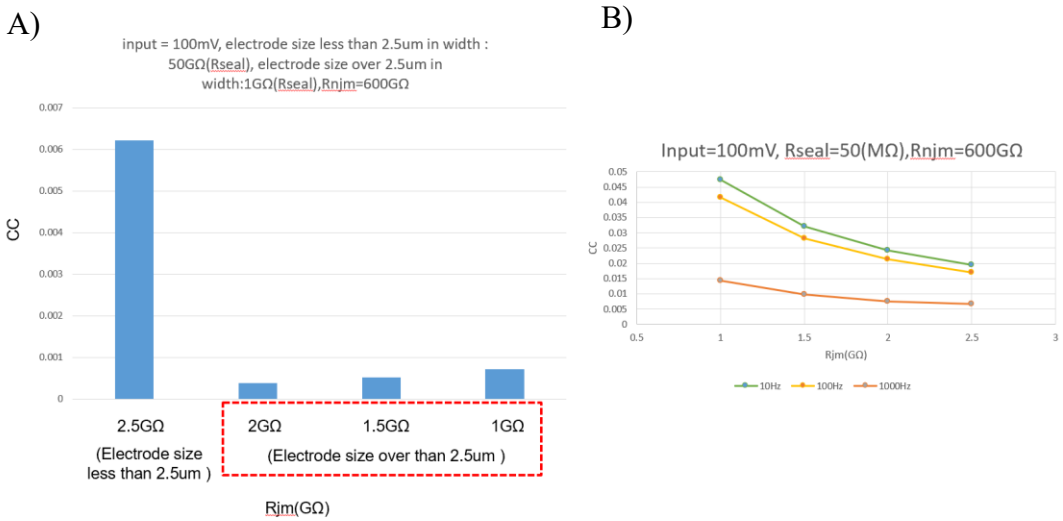

Fig. 41. A depicts that when the width of the electrode is greater than 2.5 um, there is no Rseal, and the variation in CC occurs as a result. B depicts the CC as Rjm decreases as the size of the electrode increases, in the presence of Rseal.

Fig. 41 shows that a trend different from that observed in Fig. 40-C occurs when the size of the electrode is arbitrarily increased. Therefore, it is necessary to increase the surface area of the electrode while preserving the wrapping of synapses.

In my simulation, there were many elements that could affect the CC, and the influence of Rseal on CC was the most intuitive. The results of Fig. 40-D show that the CC of 10 frequency and 100 frequency increased as Rseal increased. However, at a frequency of 1000, which is an action potential, i found that the CC value hardly changed. Therefore, improving the electrode is indicated as the way to increase the CC value, rather than reducing the synaptic gap.

I investigated the environment where the value of CC could be increased by adjusting various parameters. I deduced two ideas. One idea is to decrease Rjm. Theoretically, the way to reduce Rjm is to increase Rnjm (input resistance) or surface area. However, Fig. 40-B showed that Rnjm did not have a significant effect on increasing CC. So, I focused on the shape of the electrode. It is speculated that if the surface area is improved while keeping the size of the electrode the same, the CC can be improved. Another idea is to increase Rseal. Therefore, it can be concluded that the way to increase Rseal is to reduce the gap between the formation of synapses between neurons and electrodes. As a result, it is necessary to improve the synapse organizers. However, if only Rseal is increased, the change in CC will be insignificant. Therefore, it is necessary to find a way to improve both Rseal and Rjm simultaneously.

Chapter 5 Conclusion

This study aims to establish a new electrophysiology technique that has not been attempted before. The study was conducted in three chapters to develop this new technique.

Chapter 2 focused on the fabrication of MEA (microelectrode array) and protein adsorption. Through much effort, electrodes with a size of 2 μm or less were successfully fabricated, as shown in Fig. 20-B and D. Since the electrodes were smaller than the presynaptic structure of axon terminal, it was expected that they would induce wrapping from the presynaptic, resulting in the formation of a high Rseal and the ability to measure the action potential of the presynaptic.

In addition, experiments were conducted on protein adsorption to ensure a stable and constant amount of protein was adsorbed onto the surface. The results showed that using pulse-type voltage for adsorption resulted in more stable adsorption than the conventional method using DC voltage. However, achieving consistent protein adsorption was not always possible, even with the pulse-type method. In particular, this study is necessary because it is impossible to determine whether the cause of poor results after neuron experiments is the absence of a synapse organizer. Therefore, it is necessary to increase the binding success rate between proteins to some extent.

Chapter 3 deals with the functionalization of electrodes with synapse organizers. I checked protein binding at each step and successfully crosslinked using DSS reagent (Fig.34-C). The formation of synapses by the synapse organizer between the electrode and nerve cell was confirmed through anti-Synaptophysin antibody (Fig.36), indicating

that my new electrophysiology technique is working as expected.

However, these results were not always obtained. The main problem was protein adsorption. The efficiency of protein adsorption varied depending on the conditions. We increased the number of electrodes to improve the protein adsorption rate, but this was not a complete solution. Further protein-related experiments are needed.

Chapter 4 evaluated the performance of the current electrode and identified areas for improvement. The results in Fig. 41 showed that the current electrode could only record 0.98% of the action potentials of neurons. This result was unsatisfactory as the frequency was outside the domain of action potentials, making it difficult actually to record. However, simulations helped identify the parameters that needed improvement: Rseal and Rjm. The results showed that CC (coupling coefficient) increased when Rjm was lowered or Rseal was increased.

In conclusion, this study successfully introduced protein-specific inductive properties to MEAs. The experiment demonstrated that the common limitations of conventional electrophysiology techniques using microelectrodes can be overcome. A new technique of introducing synapse organizers into electrodes was proposed and a stable method was established. These findings suggest that in future electrophysiological experiments using microelectrodes, long-term observation and analysis can be achieved through an extracellular recording by selectively targeting specific types of cells. Additionally, this technique has potential applications in electrophysiology, neurophysiology, and even the medical field. Furthermore, the same lab is experimenting with making synapse

organizers respond to specific targets, indicating that large-scale parallel measurement through more accurate targeting will be possible in the future.

However, this study has not yet reached the stage of recording action potentials with actual neurons. My next goal is to address these challenges. Currently, mushroom-shaped electrodes are being introduced and experimented with to overcome these problems. Mushroom electrodes provide a larger surface area while retaining the size of conventional electrodes, suggesting that Rjm can be reduced while maintaining the original Rseal. Nonetheless, several issues need to be addressed before conducting experiments with neurons, and further research is needed to overcome these challenges.

Reference

[1] M. Scanziani and M. Häusser, "Electrophysiology in the age of light," *Nature*, vol. 461, no. 7266, pp. 930–939, 2009, doi: 10.1038/nature08540.

[2] M. Bresadola, "Medicine and science in the life of Luigi Galvani (1737-1798)," *Brain Res. Bull.*, vol. 46, no. 5, pp. 367–380, 1998, doi: 10.1016/S0361-9230(98)00023-9.

[3] C. L. Nguyen and J. Wayenborgh, "T He O Phthalmoscope and Some of His Other C Ontributions," pp. 165–177, 2015.

[4] R. H. Adrian and L. D. Peachey, "Reconstruction of the action potential of frog sartorius muscle," *J. Physiol.*, vol. 235, no. 1, pp. 103–131, 1973, doi: 10.1113/jphysiol.1973.sp010380.

[5] B. L. Ginsborg, "of Biophysics, University," 1958.

[6] P. W. Gage and R. S. Eisenberg, "Action potentials without contraction in frog skeletal muscle fibers with disrupted transverse tubules," *Science (80-.).*, vol. 158, no. 3809, pp. 1702–1703, 1967, doi: 10.1126/science.158.3809.1702.

[7] A. J. Pappano, "Calcium-dependent action potentials produced by catecholamines in guinea pig atrial muscle fibers depolarized by potassium.," *Circ. Res.*, vol. 27, no. 3, pp. 379–390, 1970, doi: 10.1161/01.RES.27.3.379.

[8] J. L. Mostwin, "The action potential of guinea pig bladder smooth muscle," *J. Urol.*, vol. 135, no. 6, pp. 1299–1303, 1986, doi: 10.1016/S0022-5347(17)46079-4.

[9] A. D. Wickenden, "Overview of electrophysiological techniques," *Curr. Protoc. Pharmacol.*, no. SUPPL.64, pp. 1–17, 2014, doi: 10.1002/0471141755.ph1101s64.

[10] G. Ruffini *et al.*, "First human trials of a dry electrophysiology sensor using a carbon nanotube array interface," *Sensors Actuators, A Phys.*, vol. 144, no. 2, pp. 275–279, 2008, doi: 10.1016/j.sna.2008.03.007.

[11] S. Anand and R. K. Keetha Manjari, "FPGA implementation of artificial Neural Network for forest fire detection in wireless Sensor Network," *Proc. 2017 2nd Int. Conf. Comput. Commun. Technol. ICCCT 2017*, pp. 265–270, 2017, doi: 10.1109/ICCCT2.2017.7972284.

[12] N. C. Spitzer, P. A. Kingston, T. J. Manning, and M. W. Conklin, "Outside and in: Development of neuronal excitability," *Curr. Opin. Neurobiol.*, vol. 12, no. 3, pp. 315–323, 2002, doi: 10.1016/S0959-4388(02)00330-6.

[13] E. M. Novikova, V. A. Vodeneev, and V. S. Sukhov, “Mathematical model of action potential in higher plants with account for the involvement of vacuole in the electrical signal generation,” *Biochem. Suppl. Ser. A Membr. Cell Biol.*, vol. 11, no. 2, pp. 151–167, 2017, doi: 10.1134/S1990747817010068.

[14] J. F. Atherton, D. L. Wokosin, S. Ramanathan, and M. D. Bevan, “Autonomous initiation and propagation of action potentials in neurons of the subthalamic nucleus,” *J. Physiol.*, vol. 586, no. 23, pp. 5679–5700, 2008, doi: 10.1113/jphysiol.2008.155861.

[15] A. Goel and D. V. Buonomano, “Timing as an intrinsic property of neural networks: Evidence from in vivo and in vitro experiments,” *Philos. Trans. R. Soc. B Biol. Sci.*, vol. 369, no. 1637, 2014, doi: 10.1098/rstb.2012.0460.

[16] A. Hodgkin and A. Huxley, “A quantitative description of membrane current and its application to conductance and excitation,” *J. Physiol.*, vol. 117, pp. 500–44, 1952.

[17] B. Principles, “Modern Techniques in Chemistry :,” *Molecules*, vol. 201, no. March, pp. 65–74, 2001.

[18] A. F. M. Johnstone, G. W. Gross, D. G. Weiss, O. H. U. Schroeder, A. Gramowski, and T. J. Shafer, “Microelectrode arrays: A physiologically based neurotoxicity testing platform for the 21st century,” *Neurotoxicology*, vol. 31, no. 4, pp. 331–350, 2010, doi: 10.1016/j.neuro.2010.04.001.

[19] J. Dragas *et al.*, “In Vitro Multi-Functional Microelectrode Array Featuring 59 760 Electrodes, 2048 Electrophysiology Channels, Stimulation, Impedance Measurement, and Neurotransmitter Detection Channels,” *IEEE J. Solid-State Circuits*, vol. 52, no. 6, pp. 1576–1590, 2017, doi: 10.1109/JSSC.2017.2686580.

[20] D. Zhang, “Patch clamp: A powerful technique for studying the mechanism of acupuncture,” *Evidence-based Complement. Altern. Med.*, vol. 2012, 2012, doi: 10.1155/2012/534219.

[21] G. H. Kim *et al.*, “Recent progress on microelectrodes in neural interfaces,” *Materials (Basel).*, vol. 11, no. 10, 2018, doi: 10.3390/ma11101995.

[22] E. Neher and B. Sakmann, “Single-channel currents recorded from membrane of denervated frog muscle fibres,” *Nature*, vol. 260, no. 5554, pp. 799–802, 1976, doi: 10.1038/260799a0.

[23] J. E. Tyrrell, M. G. Boutelle, and A. J. Campbell, “Measurement of Electrophysiological Signals In Vitro Using High-Performance Organic Electrochemical Transistors,” *Adv. Funct. Mater.*, vol. 31, no. 1, pp. 1–12, 2021, doi: 10.1002/adfm.202007086.

[24] B. Renshaw, A. Forbes, and B. R. Morison, “Activity of Isocortex and Hippocampus: Electrical Studies With Micro-Electrodes,” *J. Neurophysiol.*, vol. 3, no. 1, pp. 74–105, 1940, doi: 10.1152/jn.1940.3.1.74.

[25] M. E. Spira and A. Hai, “Multi-electrode array technologies for neuroscience and cardiology,” *Nat. Nanotechnol.*, vol. 8, no. 2, pp. 83–94, 2013, doi: 10.1038/nnano.2012.265.

[26] T. Tansey, “Women and the early journal of physiology,” *J. Physiol.*, vol. 593, no. 2, pp. 347–350, 2015, doi: 10.1113/jphysiol.2014.288258.

[27] J. Müller *et al.*, “High-resolution CMOS MEA platform to study neurons at subcellular, cellular, and network levels,” *Lab Chip*, vol. 15, no. 13, pp. 2767–2780, 2015, doi: 10.1039/c5lc00133a.

[28] B. J. Dworak and B. C. Wheeler, “Novel MEA platform with PDMS microtunnels enables the detection of action potential propagation from isolated axons in culture,” *Lab Chip*, vol. 9, no. 3, pp. 404–410, 2009, doi: 10.1039/b806689b.

[29] X. J. Huang, A. M. O’Mahony, and R. G. Compton, “Microelectrode arrays for electrochemistry: Approaches to fabrication,” *Small*, vol. 5, no. 7, pp. 776–788, 2009, doi: 10.1002/smll.200801593.

[30] B. Ghane-Motlagh and M. Sawan, “Design and Implementation Challenges of Microelectrode Arrays: A Review,” *Mater. Sci. Appl.*, vol. 04, no. 08, pp. 483–495, 2013, doi: 10.4236/msa.2013.48059.

[31] J. T. Fourkas, “Nanoscale photolithography with visible light,” *J. Phys. Chem. Lett.*, vol. 1, no. 8, pp. 1221–1227, 2010, doi: 10.1021/jz1002082.

[32] P. Wipt and K. M. George, “基因的改变NIH Public Access,” *Bone*, vol. 23, no. 1, pp. 1–7, 2008.

[33] K. Nakanishi, T. Sakiyama, and K. Imamura, “On the adsorption of proteins on solid surfaces, a common but very complicated phenomenon,” *J. Biosci. Bioeng.*, vol. 91, no. 3, pp. 233–244, 2001, doi: 10.1016/S1389-1723(01)80127-4.

[34] Z. O. Repository, “Title : Understanding Protein Adsorption Phenomena at Solid Surfaces Authors : Michael Rabe , Dorinel Verdes , Stefan Seeger * Address : Institute of Physical Chemistry , University of Zurich , Winterthurerstrasse 190 ,” vol. 162, pp. 87–106, 2011.

[35] J. Sagiv, “Organized Monolayers by Adsorption. 1. Formation and Structure of Oleophobic Mixed Monolayers on Solid Surfaces,” *J. Am. Chem. Soc.*, vol. 102, no. 1, pp. 92–98, 1980, doi: 10.1021/ja00521a016.

[36] D. Bobb-Semple, K. L. Nardi, N. Draeger, D. M. Hausmann, and S. F. Bent, "Area-Selective Atomic Layer Deposition Assisted by Self-Assembled Monolayers: A Comparison of Cu, Co, W, and Ru," *Chem. Mater.*, vol. 31, no. 5, pp. 1635–1645, 2019, doi: 10.1021/acs.chemmater.8b04926.

[37] M. Rabe, D. Verdes, and S. Seeger, "Understanding protein adsorption phenomena at solid surfaces," *Adv. Colloid Interface Sci.*, vol. 162, no. 1–2, pp. 87–106, 2011, doi: 10.1016/j.cis.2010.12.007.

[38] D. T. Kim, H. W. Blanch, and C. J. Radke, "Direct imaging of lysozyme adsorption onto mica by atomic force microscopy," *Langmuir*, vol. 18, no. 15, pp. 5841–5850, 2002, doi: 10.1021/la0256331.

[39] K. Kubiak-Ossowska, M. Cwieka, A. Kaczynska, B. Jachimska, and P. A. Mulheran, "Lysozyme adsorption at a silica surface using simulation and experiment: Effects of pH on protein layer structure," *Phys. Chem. Chem. Phys.*, vol. 17, no. 37, pp. 24070–24077, 2015, doi: 10.1039/c5cp03910j.

[40] S. M. Daly, T. M. Przybycien, and R. D. Tilton, "Coverage-dependent orientation of lysozyme adsorbed on silica," *Langmuir*, vol. 19, no. 9, pp. 3848–3857, 2003, doi: 10.1021/la026690x.

[41] H. Takahashi and A. M. Craig, "Protein tyrosine phosphatases PTPδ, PTPς, and LAR: Presynaptic hubs for synapse organization," *Trends Neurosci.*, vol. 36, no. 9, pp. 522–534, 2013, doi: 10.1016/j.tins.2013.06.002.

[42] T. C. Südhof, "Synaptic Neurexin Complexes: A Molecular Code for the Logic of Neural Circuits," *Cell*, vol. 171, no. 4, pp. 745–769, 2017, doi: 10.1016/j.cell.2017.10.024.

[43] T. J. Siddiqui and A. M. Craig, "Synaptic organizing complexes," *Curr. Opin. Neurobiol.*, vol. 21, no. 1, pp. 132–143, 2011, doi: 10.1016/j.conb.2010.08.016.

[44] U. M. D. E. C. D. E. Los, "The molecular biology of axon guidance."

[45] T. Yoshida *et al.*, "IL-1 receptor accessory protein-like 1 associated with mental retardation and autism mediates synapse formation by trans-synaptic interaction with protein tyrosine phosphatase δ," *J. Neurosci.*, vol. 31, no. 38, pp. 13485–13499, 2011, doi: 10.1523/JNEUROSCI.2136-11.2011.

[46] G. li Ming, H. jun Song, B. Berninger, N. Inagaki, M. Tessier-Lavigne, and P. Mu-Ming, "Phospholipase C-γ and phosphoinositide 3-kinase mediate cytoplasmic signaling in nerve growth cone guidance," *Neuron*, vol. 23, no. 1, pp. 139–148, 1999, doi: 10.1016/S0896-6273(00)80760-6.

[47] Y. Xu and G. J. Fisher, "Receptor type protein tyrosine phosphatases (RPTPs) - Roles in signal transduction and human disease," *J. Cell Commun. Signal.*, vol. 6,

no. 3, pp. 125–138, 2012, doi: 10.1007/s12079-012-0171-5.

[48] J. Woo *et al.*, “Trans-synaptic adhesion between NGL-3 and LAR regulates the formation of excitatory synapses,” *Nat. Neurosci.*, vol. 12, no. 4, pp. 428–437, 2009, doi: 10.1038/nn.2279.

[49] M. J. Chagnon, N. Uetani, and M. L. Tremblay, “Functional significance of the LAR receptor protein tyrosine phosphatase family in development and diseases,” *Biochem. Cell Biol.*, vol. 82, no. 6, pp. 664–675, 2004, doi: 10.1139/o04-120.

[50] C. E. Rasmussen and D. J. Willshaw, “Biological Cybernetics for the development of neuromuscular connections,” *Biol. Cybern.*, vol. 419, pp. 409–419, 1993.

[51] J. Sevillano, M. G. Sánchez-alonso, J. Pizarro-delgado, and M. del P. Ramos-álvarez, “Role of receptor protein tyrosine phosphatases (RPTPs) in insulin signaling and secretion,” *Int. J. Mol. Sci.*, vol. 22, no. 11, 2021, doi: 10.3390/ijms22115812.

[52] S. E. D’Souza, M. H. Ginsberg, T. A. Burke, S. C. T. Lam, and E. F. Plow, “Localizaion of an Arg-Gly-Asp recognition site within an integrin adhesion receptor,” *Science (80-.).*, vol. 242, no. 4875, pp. 91–93, 1988, doi: 10.1126/science.3262922.

[53] J. T. Corthell, “Immunoprecipitation,” *Basic Mol. Protoc. Neurosci. Tips, Tricks, Pitfalls*, pp. 77–81, 2014, doi: 10.1016/b978-0-12-801461-5.00008-3.

[54] M. Lagardère, A. Drouet, M. Sainlos, and O. Thoumine, “High-Resolution Fluorescence Imaging Combined With Computer Simulations to Quantitate Surface Dynamics and Nanoscale Organization of Neuroligin-1 at Synapses,” *Front. Synaptic Neurosci.*, vol. 14, no. April, 2022, doi: 10.3389/fnsyn.2022.835427.

[55] M. Uchigashima, A. Cheung, and K. Futai, “Neuroligin-3: A Circuit-Specific Synapse Organizer That Shapes Normal Function and Autism Spectrum Disorder-Associated Dysfunction,” *Front. Mol. Neurosci.*, vol. 14, no. October, pp. 1–22, 2021, doi: 10.3389/fnmol.2021.749164.

[56] S. F. Cogan, “Neural stimulation and recording electrodes,” *Annu. Rev. Biomed. Eng.*, vol. 10, pp. 275–309, 2008, doi: 10.1146/annurev.bioeng.10.061807.160518.

[57] I. L. Jones, P. Livi, M. K. Lewandowska, M. Fiscella, B. Roscic, and A. Hierlemann, “The potential of microelectrode arrays and microelectronics for biomedical research and diagnostics,” *Anal. Bioanal. Chem.*, vol. 399, no. 7, pp. 2313–2329, 2011, doi: 10.1007/s00216-010-3968-1.

[58] M. Morishima and Y. Kawaguchi, “Recurrent connection patterns of corticostriatal pyramidal cells in frontal cortex,” *J. Neurosci.*, vol. 26, no. 16, pp. 4394–4405, 2006, doi: 10.1523/JNEUROSCI.0252-06.2006.

[59] T. K. Hensch, “Critical period plasticity in local cortical circuits,” *Nat. Rev. Neurosci.*, vol. 6, no. 11, pp. 877–888, 2005, doi: 10.1038/nrn1787.

[60] A. Hai, J. Shappir, and M. E. Spira, “Long-term, multisite, parallel, in-cell recording and stimulation by an array of extracellular microelectrodes,” *J. Neurophysiol.*, vol. 104, no. 1, pp. 559–568, 2010, doi: 10.1152/jn.00265.2010.

[61] J. V. Le Bé and H. Markram, “Spontaneous and evoked synaptic rewiring in the neonatal neocortex,” *Proc. Natl. Acad. Sci. U. S. A.*, vol. 103, no. 35, pp. 13214–13219, 2006, doi: 10.1073/pnas.0604691103.

[62] M. E. J. Obien, K. Deligkaris, T. Bullmann, D. J. Bakkum, and U. Frey, “Revealing neuronal function through microelectrode array recordings,” *Front. Neurosci.*, vol. 9, no. JAN, p. 423, 2015, doi: 10.3389/fnins.2014.00423.

[63] M. S. Fee, P. P. Mitra, and D. Kleinfeld, “Automatic sorting of multiple unit neuronal signals in the presence of anisotropic and non-Gaussian variability.[Erratum appears in J Neurosci Methods 1997 Feb;71(2):233],” *J. Neurosci. Methods*, vol. 69, no. 2, pp. 175–188, 1996, [Online]. Available: http://ovidsp.ovid.com/ovidweb.cgi?T=JS&CSC=Y&NEWS=N&PAGE=fulltext&D=med4&AN=8946321%5Cnhttp://sirius.library.unsw.edu.au:9003/sfx_local?sid=OVID:medline&id=pmid:8946321&id=doi:&issn=0165-0270&isbn=&volume=69&issue=2&spage=175&pages=175-88&date=1996&title.

[64] S. Shoham, M. R. Fellows, and R. A. Normann, “Robust, automatic spike sorting using mixtures of multivariate t-distributions,” *J. Neurosci. Methods*, vol. 127, no. 2, pp. 111–122, 2003, doi: 10.1016/S0165-0270(03)00120-1.

[65] C. Yang, Y. Yuan, and J. Si, “High performance spike detection and sorting using neural waveform phase information and SOM clustering,” *Proc. Int. Jt. Conf. Neural Networks*, 2010, doi: 10.1109/IJCNN.2010.5596908.

[66] N. Shmoel, N. Rabieh, S. M. Ojovan, H. Erez, E. Maydan, and M. E. Spira, “Multisite electrophysiological recordings by self-assembled loose-patch-like junctions between cultured hippocampal neurons and mushroom-shaped microelectrodes,” *Sci. Rep.*, vol. 6, no. January, pp. 1–11, 2016, doi: 10.1038/srep27110.

[67] T. K. Berger, R. Perin, G. Silberberg, and H. Markram, “Frequency-dependent disynaptic inhibition in the pyramidal network: A ubiquitous pathway in the developing rat neocortex,” *J. Physiol.*, vol. 587, no. 22, pp. 5411–5425, 2009,

doi: 10.1113/jphysiol.2009.176552.

[68] P. Wijdenes, H. Ali, R. Armstrong, W. Zaidi, C. Dalton, and N. I. Syed, “A novel bio-mimicking, planar nano-edge microelectrode enables enhanced long-term neural recording,” *Sci. Rep.*, vol. 6, pp. 1–8, 2016, doi: 10.1038/srep34553.

[69] A. Fendyur, N. Mazurski, J. Shappir, and M. E. Spira, “Formation of essential ultrastructural interface between cultured hippocampal cells and gold mushroom-shaped MEA- towards ‘IN-CELL’ recordings from vertebrate neurons,” *Front. Neuroeng.*, vol. 4, no. NOVEMBER, pp. 1–14, 2011, doi: 10.3389/fneng.2011.00014.

[70] B. Eversmann *et al.*, “A 128 × 128 CMOS Biosensor Array for Extracellular Recording of Neural Activity,” *IEEE J. Solid-State Circuits*, vol. 38, no. 12, pp. 2306–2317, 2003, doi: 10.1109/JSSC.2003.819174.

[71] N. Rabieh, S. M. Ojovan, N. Shmoel, H. Erez, E. Maydan, and M. E. Spira, “On-chip, multisite extracellular and intracellular recordings from primary cultured skeletal myotubes,” *Sci. Rep.*, vol. 6, no. November, pp. 1–15, 2016, doi: 10.1038/srep36498.

[72] B. M. Schmitt and H. Koepsell, “An improved method for real-time monitoring of membrane capacitance in Xenopus laevis oocytes,” *Biophys. J.*, vol. 82, no. 3, pp. 1345–1357, 2002, doi: 10.1016/S0006-3495(02)75490-8.

[73] E. C. Reverdin and R. Weingart, “Electrical properties of the gap junctional membrane studied in rat liver cell pairs,” *Am. J. Physiol. - Cell Physiol.*, vol. 254, no. 2, pp. 226–234, 1988, doi: 10.1152/ajpcell.1988.254.2.c226.

[74] W. Hu and B. P. Bean, “Differential Control of Axonal and Somatic Resting Potential by Voltage-Dependent Conductances in Cortical Layer 5 Pyramidal Neurons,” *Neuron*, vol. 97, no. 6, pp. 1315-1326.e3, 2018, doi: 10.1016/j.neuron.2018.02.016.

[75] J. W. Um, “Roles of Glial Cells in Sculpting Inhibitory Synapses and Neural Circuits,” vol. 10, no. November, pp. 1–8, 2017, doi: 10.3389/fnmol.2017.00381.

[76] E. J. Williams, R. J. Johnston, and J. Dainty, “The electrical resistance and capacitance of the membranes of Nitella translucens,” *J. Exp. Bot.*, vol. 15, no. 1, pp. 1–14, 1964, doi: 10.1093/jxb/15.1.1.

[77] U. Ashery, R. Penner, and M. E. Spira, “Acceleration of membrane recycling by axotomy of cultured aplysia neurons,” *Neuron*, vol. 16, no. 3, pp. 641–651, 1996, doi: 10.1016/S0896-6273(00)80083-5.

[78] R. Weis and P. Fromherz, “Frequency dependent signal transfer in neuron transistors,” *Phys. Rev. E - Stat. Physics, Plasmas, Fluids, Relat. Interdiscip.*

Top., vol. 55, no. 1, pp. 877–889, 1997, doi: 10.1103/PhysRevE.55.877.